AD-A186 126 AN ANALYSIS OF APPARENT-MOTION VECTORS IN AND THE STRUCTURE OF A MID-LATI..(U) AIR FORCE INST OF TECH WRIGHT-PATTERSON AFB OH T D HALDERMAN 1987 1/2

UNCLASSIFIED AFIT/CI/NR-87-102T F/G 4/2 NL

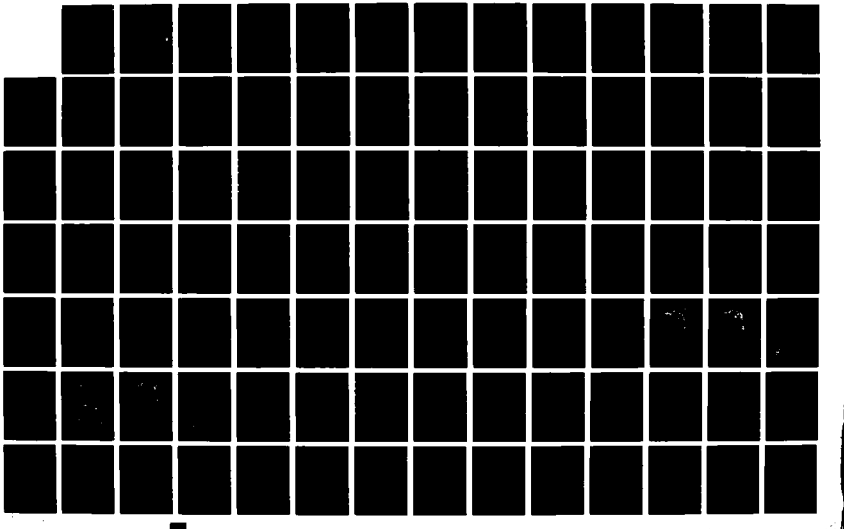

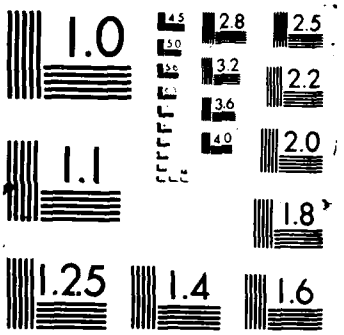
1.0
1.1
1.25
1.4
1.6
1.8
2.0
2.2
2.5
2.8
3.2
3.6
4.0
4.5
5.0

UNCLASSIFIED
SECURITY CLASSIFICATION OF THIS PAGE (When Data Entered)

REPORT DOCUMENTATION PAGE

READ INSTRUCTIONS BEFORE COMPLETING FORM

1. REPORT NUMBER: AFIT/CI/NR 87-102T
2. GOVT ACCESSION NO.
3. RECIPIENT'S CATALOG NUMBER

4. TITLE (and Subtitle): An Analysis Of Apparent-Motion Vectors In, And The Structure Of, A Mid-Latitude Sporadic E Layer Using A 2.66 MHZ Radar
5. TYPE OF REPORT & PERIOD COVERED: THESIS/DISSERTATION
6. PERFORMING ORG. REPORT NUMBER

7. AUTHOR(s): Timothy D. Halderman
8. CONTRACT OR GRANT NUMBER(s)

9. PERFORMING ORGANIZATION NAME AND ADDRESS: AFIT STUDENT AT: Utah State University
10. PROGRAM ELEMENT, PROJECT, TASK AREA & WORK UNIT NUMBERS

11. CONTROLLING OFFICE NAME AND ADDRESS: AFIT/NR, WPAFB OH 45433-6583
12. REPORT DATE: 1987
13. NUMBER OF PAGES: 89

14. MONITORING AGENCY NAME & ADDRESS (if different from Controlling Office)
15. SECURITY CLASS. (of this report): UNCLASSIFIED
15a. DECLASSIFICATION DOWNGRADING SCHEDULE

16. DISTRIBUTION STATEMENT (of this Report)

APPROVED FOR PUBLIC RELEASE; DISTRIBUTION UNLIMITED

DTIC ELECTE NOV 2 0 1987 D

17. DISTRIBUTION STATEMENT (of the abstract entered in Block 20, if different from Report)

18. SUPPLEMENTARY NOTES

APPROVED FOR PUBLIC RELEASE: IAW AFR 190-1

LYNN E. WOLAVER 23 Nov 87
Dean for Research and Professional Development
AFIT/NR

19. KEY WORDS (Continue on reverse side if necessary and identify by block number)

20. ABSTRACT (Continue on reverse side if necessary and identify by block number)

ATTACHED

DD FORM 1 JAN 73 1473 EDITION OF 1 NOV 65 IS OBSOLETE

SECURITY CLASSIFICATION OF THIS PAGE (When Data Entered)

87 10 28 164

102

AN ANALYSIS OF APPARENT-MOTION VECTORS IN, AND THE STRUCTURE OF, A MID-LATITUDE SPORADIC E LAYER USING A 2.66 MHZ RADAR

by

Timothy D. Halderman

A thesis submitted in partial fulfillment
of the requirements for the degree

of

MASTER OF SCIENCE

in

Soil Science and Biometeorology

(Aeronomy)

Approved:

Major Professor

Committee Member

Committee Member

Committee Member

Dean of Graduate Studies

UTAH STATE UNIVERSITY
Logan, Utah

1987

ABSTRACT

An Analysis of Apparent-Motion Vectors in, and the Structure of, a Mid-Latitude Sporadic E Layer using a 2.66 MHz Radar

by

Timothy Dayton Halderman, Master of Science

Utah State University, 1987

Major Professor: Dr. Gene W. Adams
Department: Soil Science and Biometeorology

We used the 2.66 MHz Imaging Middle-Atmosphere Geophysical Radar (IMAGER) located at Boot Lake, Colorado, to collect data on mid-latitude sporadic E layers found near 100 km. Analysis of the data shows apparent-motion vectors, in a 20 km altitude range in and near the layers, of 200-300 m/s on one occasion and 160 m/s on another. In each case, these motions were toward the west and south. We interpret these results as phase motions of internal gravity waves, or "ripples," moving through the lower thermosphere, rather than bulk wind motions. Possible lower atmosphere source regions for these internal gravity waves are identified. The sporadic E "layers" appeared to consist of irregularly shaped patches with scale sizes being approximately 15 km. The heights of the individual patches appeared to vary as much as 3 km while the mean height of the layer varied from 106 km to as low as 96 km. We also had a 5-point

tilting-filter photometer available which enabled us to calculate apparent-motions at similar altitudes. The results showed motion toward the north at approximately 100 m/s, significantly different, in both direction and speed, than the results from the radar.

(98 pages)

AN ANALYSIS OF APPARENT-MOTION VECTORS IN, AND THE STRUCTURE OF, A MID-LATITUDE SPORADIC E LAYER USING A 2.66 MHZ RADAR

by

Timothy D. Halderman

A thesis submitted in partial fulfillment
of the requirements for the degree

of

MASTER OF SCIENCE

in

Soil Science and Biometeorology

(Aeronomy)

Approved:

Major Professor

Committee Member

Committee Member

Committee Member

Dean of Graduate Studies

UTAH STATE UNIVERSITY
Logan, Utah

1987

ACKNOWLEDGMENTS

This research was supported by the Air Force Geophysical Laboratory under contract F19628-83-C-0056 as part of the MAPSTAR (Middle Atmosphere Periodic Structure, Associated Radiance) project, the National Science Foundation under grants ATM-8117275, ATM-8419810, and ATM-8608391, and by a grant from Imaging Doppler Interferometry (IDI), Inc.

That said, I thank Dr. Gene Adams for the many hours of instruction and discussion he spent with me in the course of this research. Without his suggestions and ever positive approach to sometimes confusing data results this project would never have reached this point. I would also like to thank Dr. Kent Miller, and Dr. Larry Hipps for the many excellent suggestions they made for improving the content of this report. Conversations with fellow students, Ali Ghafourian and Reese Johnson, were also of great help to me and I wish to thank them for their time as well.

I would like to thank Dr. J. W. Meriwether and Dr. A. W. Peterson for allowing me to use data collected by them at Boot Lake, Colorado and Jelm, Wyoming, respectively, prior to publication of results under their own names.

None of this would have been possible without the sponsorship of the United States Air Force through the Air Force Institute of Technology (AFIT) program. I hope someday to make a small return on their investment in me.

Last, and most importantly, I thank my wife, Helen, for the love and encouragement she has given me during our entire stay at Utah State.

Without her unfailing support I would never have completed this thesis. It will be called "my" thesis; in reality it is "our" thesis.

Timothy Dayton Halderman

TABLE OF CONTENTS

LIST OF TABLES

LIST OF FIGURES

LIST OF FIGURES CONTINUED

ABSTRACT

An Analysis of Apparent-Motion Vectors in, and the Structure of, a Mid-Latitude Sporadic E Layer using a 2.66 MHz Radar

by

Timothy Dayton Halderman, Master of Science

Utah State University, 1987

Major Professor: Dr. Gene W. Adams
Department: Soil Science and Biometeorology

We used the 2.66 MHz Imaging Middle-Atmosphere Geophysical Radar (IMAGER) located at Boot Lake, Colorado, to collect data on mid-latitude sporadic E layers found near 100 km. Analysis of the data shows apparent-motion vectors, in a 20 km altitude range in and near the layers, of 200-300 m/s on one occasion and 160 m/s on another. In each case, these motions were toward the west and south. We interpret these results as phase motions of internal gravity waves, or "ripples," moving through the lower thermosphere, rather than bulk wind motions. Possible lower atmosphere source regions for these internal gravity waves are identified. The sporadic E "layers" appeared to consist of irregularly shaped patches with scale sizes being approximately 15 km. The heights of the individual patches appeared to vary as much as 3 km while the mean height of the layer varied from 106 km to as low as 96 km. We also had a 5-point

tilting-filter photometer available which enabled us to calculate apparent-motions at similar altitudes. The results showed motion toward the north at approximately 100 m/s, significantly different, in both direction and speed, than the results from the radar.

(98 pages)

CHAPTER I

INTRODUCTION

The advent of space flight brought with it an urgent need to better understand the earth's upper atmosphere. A great deal of progress has been made in the last thirty years observationally and theoretically, but there are still many physical and chemical processes that are not yet well understood.

Processes in the upper mesosphere and lower thermosphere are especially difficult to describe for both observational and theoretical reasons. These regions are virtually inaccessible to long term direct measurement such as is possible in the lower atmosphere. Balloon and aircraft instrumentation can't reach these heights; rocketsonde lifetimes are only on the order of minutes. Remote sensing equipment such as the ionosonde and the incoherent-scatter radar have probably contributed the most toward our present understanding, but these instruments are somewhat limited in their ability to view the horizontal structure of the atmosphere. Satellites have eliminated this problem to some degree, but they are poor in terms of temporal resolution at a given point.

From a theoretical standpoint this portion of the earth's atmosphere also provides the aeronomer, the physicist, the chemist with a great challenge. He must consider charged particle motions in the earth's magnetic field, plasma-neutral particle interactions, and plasma instabilities in addition to the neutral particle motions he

may already be familiar with from study of the lower atmosphere. There is a positive side in having to consider ionized particles. The ground-based radar systems that probe the atmosphere depend on changes in the index of refraction to operate. In the lower atmosphere, changes in this index are caused primarily by variations in the pressure, temperature, or humidity of the medium. In the ionosphere, changes in the electron number density are primarily responsible for changes in the index of refraction. Radar systems then respond very well to changes in ionization and therefore can in some sense measure the ionosphere.

The researcher must also add internal gravity waves and tidal waves to his list of things to consider. At mid-latitudes, many processes exhibit 12 and 24-hour periodicities, reflecting the semi-diurnal and diurnal components of the tides. On top of this, there are many irregularities with periods of 3 hours or less that are thought to be caused by internal gravity waves, launched in the lower atmosphere, propagating through the ionosphere.

It is these short period irregularities that we focus on for the remainder of this work. In particular, we will consider apparent-motions associated with these short period disturbances.

By the time a gravity wave reaches the lower ionosphere, the wind perturbations associated with it are quite large, having grown exponentially with height in response to the exponentially decreasing number density. These winds redistribute the ionization into what is observed as an ionospheric irregularity that moves at the phase velocity of the gravity wave (Beer, 1974). This irregularity is the manifestation of the internal gravity wave moving through the ionosphere and is often called a "traveling ionospheric disturbance," or TID.

In this work, we use coincident 2.66 MHz Doppler interferometer radar and 557.7 nm atomic oxygen emission measurements to study apparent-motions in the lower E region. We use the term "apparent-motions" because there has been some debate in the past as to the interpretation of motions measured with the Doppler shift of the returned radar pulses (Adams et al., 1986b), the two alternatives being phase motions as described above or neutral wind velocities.

The Doppler interferometer also provides the capability to view the horizontal structure of the atmosphere. Here we use this capability to examine the structure of a mid-latitude sporadic E layer.

Objectives

We have chosen two days for analysis: June 24-25, 1984 and June 29-30, 1984. These particular days were chosen because sporadic E was present on each occasion for at least two consecutive hours during the observation period. This long term presence provided the ionization necessary for us to use the Doppler interferometry techniques described in Chapter III. The latter of the two days was also extremely active at optical wave-lengths throughout the night. Atomic oxygen emissions at 557.7 nm provided a second, independent method of determining apparent motions at similar altitudes. The specific objectives of this research are as follows:

1) Use Doppler interferometry analysis to determine apparent-motion vectors in the lower E region. Discuss and interpret the results in terms of neutral wind velocities and/or phase velocities associated with TIDs.

2) Examine the spatial and temporal variations of sporadic E using the scattering points identified by the Doppler interferometer.

3) Determine apparent-motion vectors from the 557.7 nm atomic oxygen emission curves and compare these results to the Doppler interferometer results.

4) Calculate and compare the spectral power densities for 557.7 nm emissions and for received power returns on the Doppler interferometer.

CHAPTER II

LITERATURE REVIEW

Traveling Ionospheric Disturbances

Hines (1960) first proposed that the many irregularities seen in the upper atmosphere were caused by acoustic-gravity waves moving through that region. In this classic paper he not only developed the dispersion relation describing these waves, he applied them to the irregular phenomena seen up to that day and showed they could, in large part, be explained by these waves. This work has been the foundation for much of the progress made in describing inonospheric irregularities. Before discussing the published results on TIDs a brief review of the properties of acoustic-gravity waves is appropriate.

The earth's atmosphere is in large part stably stratified. This means a parcel of air displaced vertically (up or down) will tend to return to that initial position. The buoyancy force is responsible for its return to the equilibrium position. When buoyancy forces are comparable in magnitude to pressure gradient forces the resulting waves are called acoustic gravity-waves.

The three basic equations describing conservation of momentum, energy, and mass are the starting point for understanding acoustic-gravity wave motions. These are given below.

$$\frac{\partial \tilde{u}}{\partial t} + \tilde{u} \cdot (\nabla \tilde{u}) = \frac{-1}{\rho} \nabla p + \tilde{g} \qquad (2.1)$$

$$\frac{\partial p}{\partial t} + \tilde{u} \cdot \nabla p = c^2 \left(\frac{\partial \rho}{\partial t} + \tilde{u} \cdot \nabla \rho\right) \tag{2.2}$$

$$\frac{\partial \rho}{\partial t} + \nabla \cdot (\rho \tilde{u}) = 0 \tag{2.3}$$

Here, p represents the atmospheric pressure, ρ the atmospheric density, $\tilde{u}$ the neutral wind velocity, and c the speed of sound. By neglecting Coriolis and viscous effects and considering only inertial, buoyancy, and pressure gradient forces, several terms have been eliminated in equations 2.1-2.3.

To further simplify we assume an isothermal, motionless atmosphere. These are rather severe restrictions, particularly in the lower thermosphere; however, the intent here is to obtain only a general understanding of gravity waves. By further assuming that perturbations are small compared to the quantities themselves, linearized forms of equations 2.1-2.3 can be written as follows:

$$\rho_o \frac{\partial u_{1x}}{\partial t} = - \frac{\partial p_i}{\partial x} \tag{2.4}$$

$$\rho_o \frac{\partial u_{1z}}{\partial t} = - \frac{\partial p_1}{\partial z} - g \rho_1 \tag{2.5}$$

$$\frac{\partial p_1}{\partial t} + u_{1z} \frac{\partial p_o}{\partial z} = c^2 \left(\frac{\partial \rho_1}{\partial t} + u_{1z} \frac{\partial \rho_o}{\partial z}\right) \tag{2.6}$$

$$\frac{\partial \rho_1}{\partial t} + u_{1z} \frac{\partial \rho_o}{\partial z} + \rho_o \left(\frac{\partial u_{1x}}{\partial x} + \frac{\partial u_{1z}}{\partial z}\right) = 0 \tag{2.7}$$

(Beer, 1974). Here the values subscripted with 1 indicate the perturbed values while those subscripted with 0 represent unperturbed quantities. Note the momentum equation has been expressed in scalar form in the x and z-directions. By neglecting Coriolis effects we are limiting the size and period of the waves considered to less than several hundred kilometers and less than about 4 hours, respectively. Waves larger than this are considered tidal motions and would be covered under tidal theory.

By assuming the perturbed quantities are varying sinusoidally such that,

$$p_1/p_0 P = \rho_1/\rho_0 R = U_{1x}/X = U_{1z}/Z = A_0 \exp[i(\omega t - K_x x - K_z z)] \quad (2.8)$$

a matrix of four linear equations in four variables (p_1/p_0, ρ_1/ρ_0, U_{1x} and U_{1z}) can be formed whose solution, when the matrix is set to zero, is given by the following:

$$\omega^4 - \omega^2 c^2 (K_x^2 + K_z^2) + (\gamma - 1)\, g^2 K_x^2 + i\gamma g\, \omega^2 K_z = 0 \quad (2.9)$$

This is the dispersion relation relating the circular wave frequency ω to the constant complex wave numbers K_x and K_z. Here, γ is the ratio of specific heats (C_p/C_v). Note, no K_y term appears in this equation because a rotation of the coordinate system such that x is in the direction of horizontal phase propagation eliminates the need for this term. The polarization terms P, R, X, and Z relate the magnitudes and phases of the changes in pressure, density, and horizontal and vertical motions. They are assumed constant and are given below:

$$P = \gamma \omega^2 K_z - i\gamma g \omega^2/c^2 \tag{2.10}$$

$$R = \omega^2 K_z + i(\gamma - 1) g K_x^2 - i\gamma g \omega^2/c^2 \tag{2.11}$$

$$X = \omega K_x K_z c^2 - i g \omega K_x \tag{2.12}$$

$$Z = \omega^3 - \omega K_x^2 c^2 \tag{2.13}$$

(Hines, 1960).

Equations 2.9-2.13 are the basis for describing the characteristics of gravity waves. First of all we note in equation 2.9 that K_x and K_z can't both be purely real and non-zero. If we assume that $K_x = k_x$ (K_x has only a real component) then K_z must have an imaginary component. The real and imaginary components of equations 2.9 are given by

$$\omega^4 - \omega^2 c^2 (k_x^2 + k_z^2) - [\mathrm{Im}(K_z)]^2 - \omega^2 \gamma \, \mathrm{Im}(K_z) + (\gamma - 1) g^2 k_x^2 = 0 \tag{2.14}$$

and

$$\omega^2 \gamma g \, \mathrm{Re}(K_z) - 2\omega^2 c^2 \mathrm{Re}(K_z) \mathrm{Im}(K_z) = 0 \tag{2.15}$$

There are two different conditions that satisfy equation 2.15, either $\mathrm{Re}(K_z) = 0$, or $\mathrm{Im}(K_z) = \gamma g/2c^2$. The first of these corresponds to the evanescent wave mode where there are no phase variations in the vertical. The second leads to the acoustic-gravity waves we are interested in looking at.

By substituting the second solution into equation 2.9, two separate frequency ranges emerge as solutions. These can be seen in the constant k_z contour graph shown in Figure 1 as the acoustic wave region where $\omega > \omega_a$, and the internal gravity wave region where $\omega < \omega_B$. The frequencies ω_a and ω_B are the acoustic cut-off frequency and the isothermal Brunt-Vaisala frequencies, respectively. These frequencies are given by

$$\omega_a = \frac{\gamma g}{2c} \tag{2.16}$$

and

$$\omega_B = \frac{(\gamma - 1)^{\frac{1}{2}} g}{c} \tag{2.17}$$

The region between these two frequencies is the evanescent mode region where $k_z = 0$. This means that gravity wave period must be greater than the Brunt-Vaisala period which is about 4 minutes in the lower thermosphere.

The group velocity ($d\omega/dk$) and phase velocity (ω/k) in the x and z-directions can be obtained from the dispersion relation (equation 2.9). We won't go through the mathematical steps or write down the equations here, but simply point out two important facts regarding these quantities. First, the horizontal phase and group velocities of a gravity wave are in the same direction while the vertical components are in opposite directions. This means if a gravity wave is propagating upward from the lower atmosphere the phase of the wave will be directed downward and radar observations of the associated irregularity would show a downward drift motion. It should also be pointed out that the horizontal and vertical phase velocities are not actually components of the total phase velocity, but are related in the following manner:

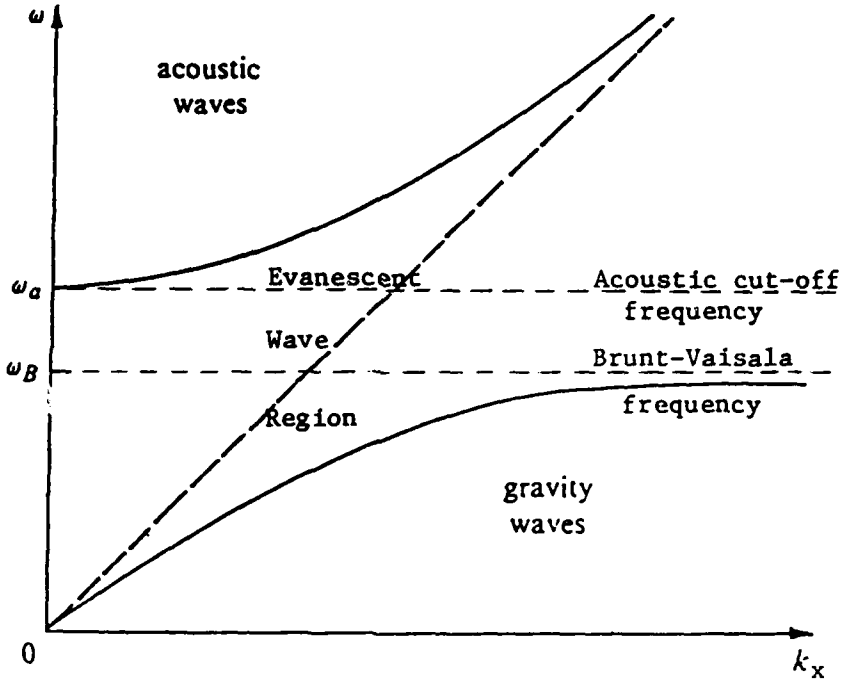

Fig. 1. Acoustic-gravity wave dispersion curves for constant k_z contours.

$$1/V_p^2 = 1/V_x^2 + 1/V_z^2 \qquad (2.18)$$

(Beer, 1974). Thus, a very large horizontal phase velocity contributes little to the total phase velocity of a wave.

A schematic diagram of a gravity wave propagating obliquely upward through the atmosphere is shown in Figure 2. The velocity perturbations perpendicular to the direction of the phase motion are responsible for driving parcels of air above and below their equilibrium positions. This in turn causes alternating areas of compression and rarefraction at the positions noted. It should also be noted the amplitude of the perturbations increases exponentially with altitude, their magnitude being estimated at approximately 50 m/s at lower thermospheric heights (Kochansky, 1964; Hines, 1966).

Francis' (1973, page 10) description sums up gravity waves and their effects succinctly:

> Putting together all of these properties, a rather peculiar picture emerges - a wave packet propagating obliquely upward containing within it transverse velocity oscillations which grow exponentially as the wave propagates, and whose phase structure propagates downward, perpendicular to the motion of the wave packet as a whole.

As a wave moves by a point in space individual parcels trace out elliptical orbits. Figure 3 illustrates the various shapes of these ellipses in the x-z plane for different values of the refractive indices (here labeled as μ) in the horizontal and vertical directions. In the figure, Y is the ratio between the isothermal value of the Brunt-Vaisala frequency and the frequency of the wave in question; the larger the value, the greater the period of the wave. Thus, we see the longer the period of the wave, the more elongated the orbit. At the

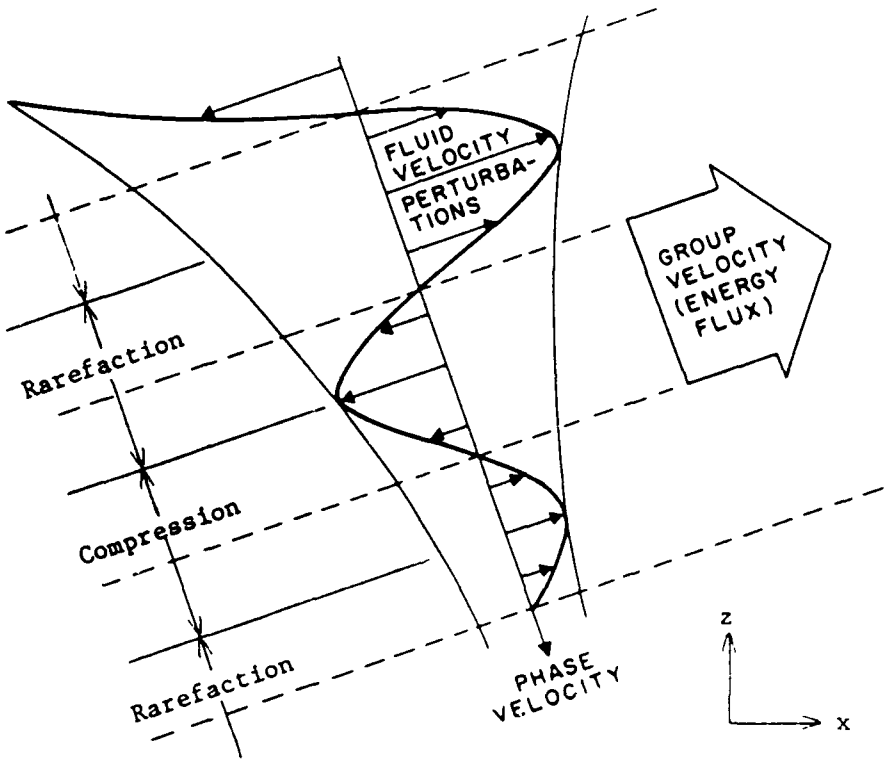

Fig. 2. Schematic representation of an internal gravity wave (adapted from Hines, 1960).

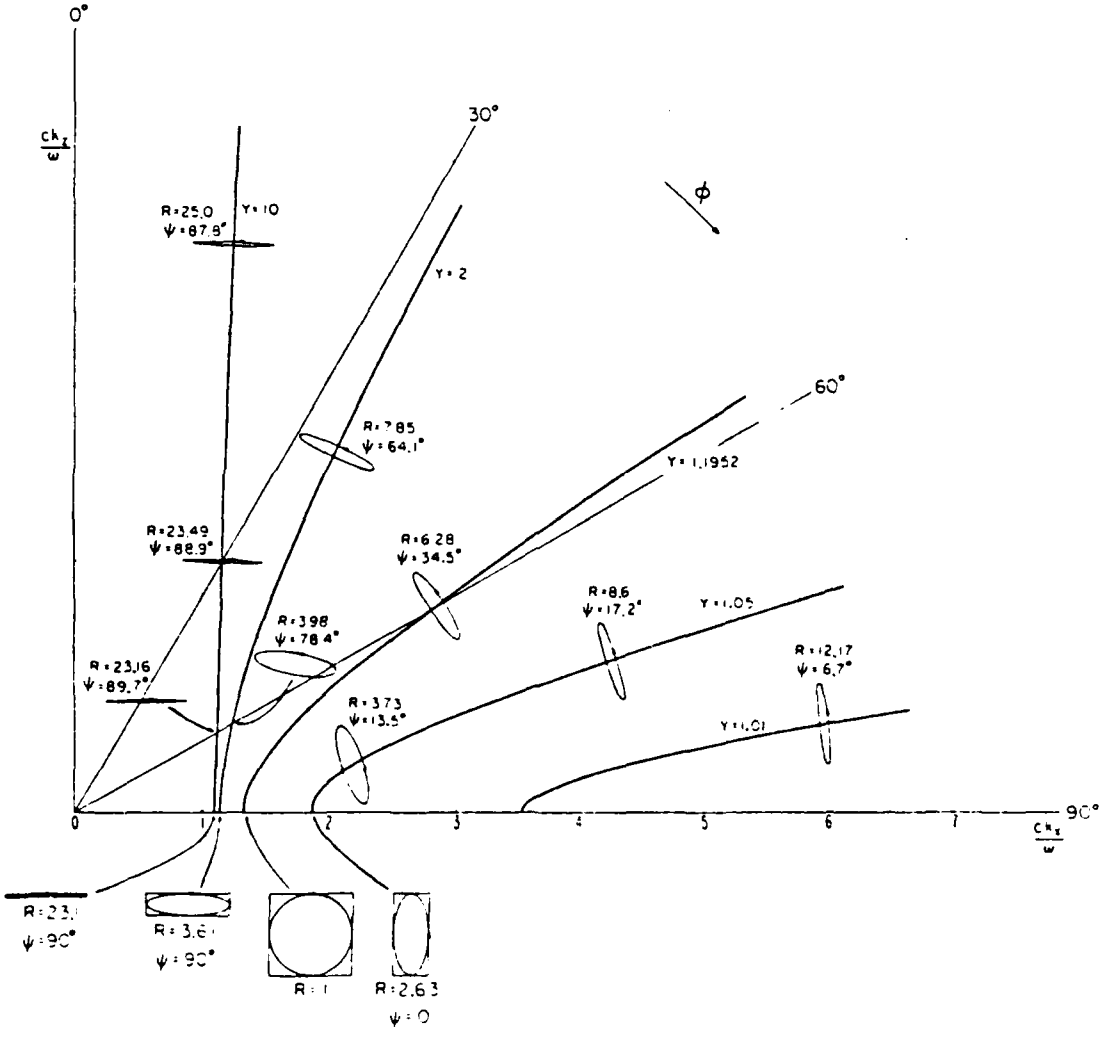

Fig. 3. Refractive index (μ) curves and parcel orbits for gravity waves in an isothermal atmosphere.

same time, the longer the period, the smaller the angle between the group velocity and the horizontal, i.e., long period gravity waves propagate nearly horizontally. At $k_z = 0$ (i.e. horizontal propagation only), the motion of the parcel is circular when $\omega = \omega_B/\sqrt{2}$. We also note for propagation in the positive x-direction the motion at the top of the ellipse is in the same direction as the direction of propagation.

The preceding discussion of gravity waves was very simplified because of the large number of assumptions made at the outset. The fact that the atmosphere is not isothermal and windless means gravity waves can be reflected, refracted, or ducted at different heights depending on the changes of these quantities with height. Neither was viscous dissipation of the wave energy considered. Critical levels exist where the phase velocity of the wave is the same as that of the background velocities. At these levels the energy of the wave is transferred to the background wind. These processes tend to restrict the number of waves reaching the lower thermosphere. The discussion of all these different processes due to variations from an isothermal atmosphere is beyond the scope of this work. Further information on these subjects can be found in the collection of Hines' work (Hines, 1974a).

Tidal waves are also quite important in the ionosphere. Their contributions to atmospheric motion are believed comparable to gravity wave effects (Hines, 1963). The equations describing these waves in the atmosphere are similar to those describing gravity waves, except Coriolis forces must be considered because of the longer time scale. In general, motions associated with the solar tides rotate clockwise

in the northern hemisphere with time on diurnal and semidurnal basis. Chapman and Lindzen (1970) offer an excellent starting point for review of tidal motions.

The speed of propagation of traveling ionospheric disturbances has been measured, using a variety of techniques, since the 1940's. Munro (1948, 1950) was the first to report short period horizontal and vertical movements in the ionosphere. He used a trio of spaced transmitters (5.8 MHz) with a receiver at one of the transmitting points to record the passage of these "disturbances" over his observation system. Since his time many others have also measured this same phenomenon using a wide variety of techniques. Table 1 provides a summary of the techniques and results seen by others. Here, the phase propagation velocity and the region where the activity was seen have been focused on rather than the periods of the gravity waves. As can be seen in Table 1, much of the early literature focused on TIDs in the F region. It is only in the last 10 years that research efforts have moved down into the E region.

To make some sense out of this seemingly random table of observations, Georges (1968) divided the results into two broad categories: Large scale traveling ionospheric disturbances (LSTIDs), and medium scale traveling ionospheric disturbances (MSTIDs). To LSTIDs he assigned the following characteristics:

1) Large horizontal wavelengths (1000 to 5000 km) and relatively long periods ($30 < \tau < 180$ min).
2) Large amplitudes, and relatively infrequent occurrences that are well correlated with geomagnetic activity.

TABLE 1. Movement of Traveling Ionospheric Disturbances

RESEARCHER	METHOD	REGION/HEMISPHERE	HORIZONTAL PHASE VELOCITY (meters/sec)	DIRECTION (Toward the . .)
Munro (1958)	Spaced 5.8 MHz Receivers	F-Region / S	115-150	Variable NE-winter ESE-summer
Chan & Villard (1962)	CW Doppler	F-Region / N	400-765	S
Thome (1964)	Thomson Back-scatter (Arecibo)	F-Region / N	50-100	S-SW
Bowman (1965)	Ionosonde	F-Region / S	361 722 (assumed)	From conj. high lat. points
Georges (1968)	CW Doppler	F-Region / N	$>$ 300 $<$ 300	S
Goodwin (1968)	Spaced Ionosondes	E-Region / S	30	NW
Titheridge (1968)	Faraday rotation of satellite signals	F-Region / S	50	N-NE
Davies & Jones (1972)	CW Doppler	Lower F-Region / N	83-224	S-winter N-summer
Vincent (1972)	MF Doppler	E-Region / S	30-160	NE
Moreels & Herse (1977)	OH Emissions	85 km / N	14.5, Stationary, 5-17	E - S
Freund & Jacka (1979)	OI Emissions (557.7 nm)	97 km / S	50-100	Variable $>$ 90° from wind

TABLE 1 (Continued). Movement of Traveling Ionospheric Disturbances

RESEARCHER	METHOD	REGION/HEMISPHERE	HORIZONTAL PHASE VELOCITY (meters/sec)	DIRECTION (Toward the . .)
Battaner & Molina (1980)	OI Emissions (557.7 nm)	97 km / N	Seasonal - 25-32 winter 60-150 summer	not reported
Armstrong (1982)	OI Emissions (557.7 nm)	95 km / S	72	S
Meek & Manson (1983)	OI Emissions (557.7 nm)	97 km / N	50-1500	Variable - 90° from wind
Vincent & Reid (1983)	MF Doppler	80-95 km / S	50	Zonal component only
Mayr et al. (1984)	Theoretical	E-Region / N & S	250, 170	Variable
Meek et al. (1985)	Spaced Wind Observations	60-110 km / N	20-100	Variable not SW, N
Tedd & Morgan (1985)	Spaced Ionosondes	F-Region / N	100-200	S-SE
Mercier (1986)	Radioastronomy	E through F Regions / N	not reported	S-SE
Waldock & Jones (1986)	CW Doppler	F-Region / N	75-250	Rotating; 130-140° from wind
Kelder & Spoelstra (1987)	TEC Measurements and Doppler	E through F Regions / N	100-200	S-W
Adams et al. (1987)	Doppler Interferometer	88 km / N	134	S

3) Fast horizontal propagation speeds ($300 < V_h < 1000$ m/s).

4) Propagation direction toward the equator.

MSTIDs are smaller in all respects with wavelengths between 100 and 500 km, periods of 15 to 60 minutes, and propagation speeds of 100 to 300 m/s.

It is apparent, if we accept this categorization, that most of the results in Table 1 fit the medium scale TID category in terms of propagation speed. Equatorward propagation of disturbances in the F region seems to be a common feature of many of the observations. Directions in the E region are much more variable and are often described as being perpendicular to the mean winds measured at the same altitude (Freund and Jacka , 1979; Meek and Manson, 1983; Meek et al., 1985; Waldock and Jones, 1986) even though several authors have shown a connection between irregularities in the two regions (Bowman, 1968; van Eyken et al., 1982).

There have been several sources proposed for gravity wave motions in the ionosphere. Weather phenomena such as large thunderstorms (Georges, 1968; Davies and Jones, 1971), surface fronts (Freund and Jacka , 1979), jetstream maxima (Hines, 1974a), large scale low pressure systems in the troposphere (Mercier, 1986), and lee waves near mountain ranges (Beer, 1974) have all been suggested. An auroral source region has also been suggested (Chan and Villard, 1962; Hunsucker and Tveten, 1967; Goodwin, 1968; Georges, 1968). This is especially attractive since many results indicate equatorward motion.

Tidal motions have also been mentioned as a source for the generation of gravity waves. Lindzen (1968) showed that the diurnal tide could become unstable in the region between 80 and 120 km. Tidal waves

propagating upward would tend to break here because the Brunt-Vaisala frequency reaches its lowest value anywhere in the atmosphere in this region. The Brunt-Vaisala frequency appears in the numerator of the Richardson number, given by

$$Ri = (\omega_B)^2/(\partial U / \partial z)^2 \qquad (2.19)$$

which is often used as an indicator for the onset of turbulence, the critical value being approximately 0.25. This mechanism would provide a continuous source for gravity waves, which supports the observations of Gross (1983) and Kelder and Spoelstra (1987). Tidally generated waves would also tend to show a rotation in the clockwise direction as was previously noted.

Formation and Structure of Mid-Latitude Sporadic E

Rocketsonde measurements, with vertical resolutions as fine as 10 meters, show that sporadic E is made up of thin layers of enhanced ionization usually between 1 and 3 km thick (Smith and Mechtly, 1972). These layers are found in the lower E region between 90 and 120 km. Sporadic implies the unpredictable occurrence of a phenomenon in time and space. This characteristic is true in both senses only for mid-latitude sporadic E (Hargreaves, 1979; Leighton et al., 1962). Here, we define mid-latitude as being greater than $\pm$ 4° magnetic dip angle and less than $\pm$ 60° magnetic latitude (Whitehead, 1970). Wind shears are thought to be the primary production mechanism for mid-latitude sporadic E. These shears are quite variable in the lower E region and thus, so is the presence of sporadic E. Equatorial sporadic E is a predictable dayside feature associated with plasma instabilities

found near the equatorial electrojet (Balsley et al., 1976). Auroral sporadic E is a common nightside feature tied to auroral precipitation (Hunsucker, 1975). This research will be limited to the study of mid-latitude sporadic E as data are available only from the Boot Lake field site near Brighton, Colorado.

Whitehead (1970) summarized and commented on the results of numerous research efforts on sporadic E. He found the horizontal extent of a sporadic E cloud varied greatly depending on the type of system used to observe the phenomenon: from a 1000 km frontal extent inferred by spaced ionosonde measurements (Goodwin, 1966) down to meter size irregularities observed by VHF radars.

Because the vertical dimension is generally such smaller than the horizontal dimension, a sporadic E "cloud" is really more like a pancake or thin layer of enhanced ionization. Within these layers, Miller and Smith (1975, 1978) clearly showed there are often smaller patches of much more intense ionization present even though these are almost never seen in rocketsonde measurements of a sporadic E layer.

As was mentioned above, the primary production mechanism for mid-latitude sporadic E is thought to be shears in the neutral wind. Figure 4 illustrates the first of two processes that can force ionization into thin layers similar in structure to observed sporadic E layers. Charged particles in the ionosphere are constrained to move along the geomagnetic field lines when their gyrofrequency is greater than their collision frequency with neutral particles. This occurs for ions at altitudes above approximately 120 km. Dungey (1956, 1959) was the first to apply this to the ionosphere. The wind component parallel to the magnetic field forces ions to converge at alternating

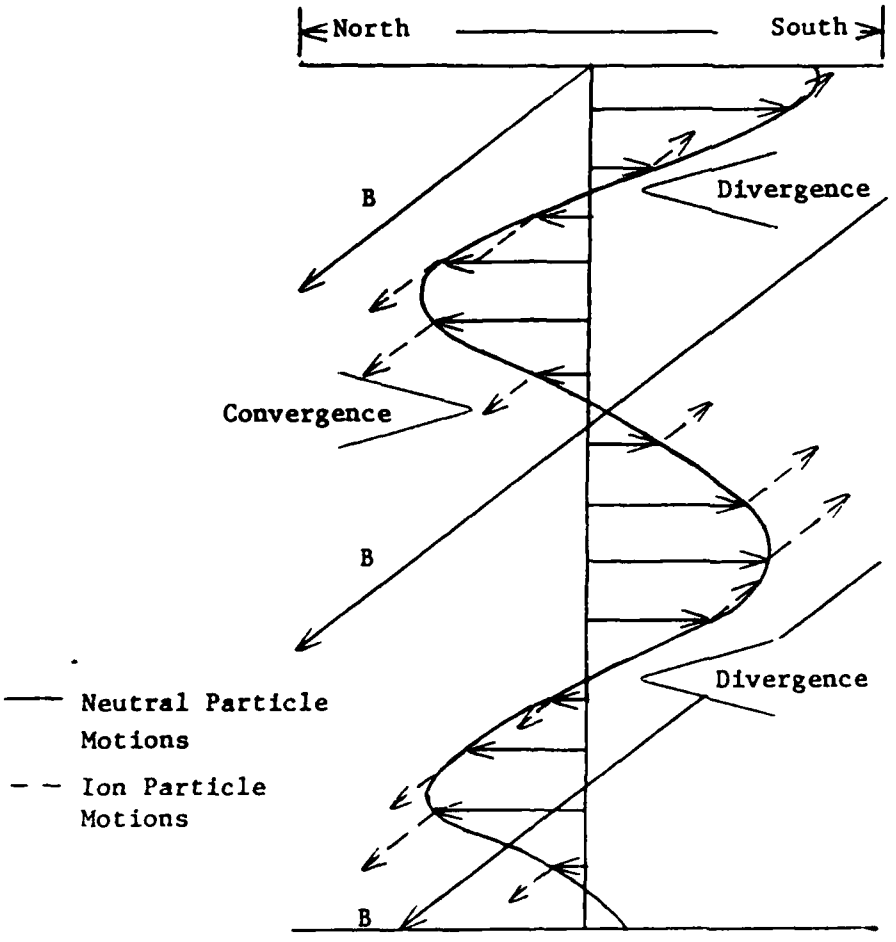

Fig. 4. Schematic of Dungey's wind shear ion convergence process.

nodes of the neutral wind. Since the horizontal component of the geomagnetic field is directed in a north-south fashion, only wind components in this direction are effective in this process.

Whitehead (1961) showed that a second, more effective wind shear convergence mechanism exists in regions where the ion-neutral collision frequency is greater than the ion gyrofrequency. Here, ions are forced to move across the magnetic field lines. In doing so they acquire a V X B drift velocity with a vertical component whose sign depends on direction of the neutral wind. Figure 5 shows how a layer of ionization is formed by this process. Note, only winds perpendicular (East-West) to the horizontal component of the geomagnetic field are effective in producing layers of ionization. Because sporadic E is seldom observed above 120 km, this process is considered the more important of the two in forming sporadic E layers.

The most concise description of the wind shear mechanism in mathematical terms is given by Miller and Smith (1978) as follows:

$$\tilde{v} = \frac{1}{1 + \rho^2} \left[\rho^2 \tilde{u} + \rho \tilde{u} \times \tilde{\Gamma} + (\tilde{u} \cdot \tilde{\Gamma}) \tilde{\Gamma} \right. \qquad (2.20)$$

where $\tilde{v}$ represents the velocity of a charged particle, Here, ρ is the ratio between the collision frequency ν and the gyrofrequency ω_H or, $\rho = \nu / \omega_H$, with the gyrofrequency being defined by $\omega_H = \frac{qB_0}{m}$. The quantity $\tilde{\Gamma}$ is the unit vector in the direction of the magnetic field and B_0 is simply the magnitude of that vector. The vector $\tilde{u}$ takes into account the neutral wind velocity $\tilde{w}$ and external electric field effects and is given by

$$\tilde{u} = \tilde{w} + \tilde{E} / \rho B_0 \qquad (2.21)$$

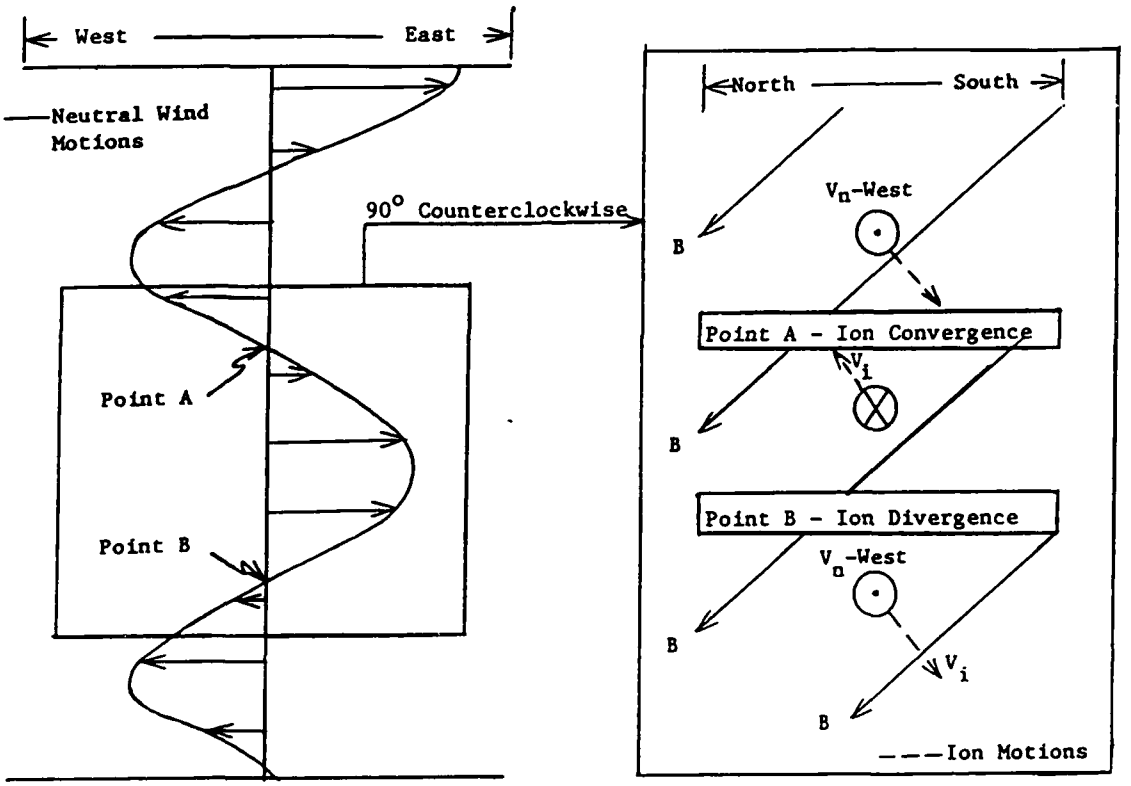

Fig. 5. Schematic of Whitehead's wind shear ion convergence process.

The relative importance of the various components of the neutral wind velocity can be seen for different altitudes from equation 2.17. Above 120 km is greater than 1 and the ions become more and more constrained to movements along the magnetic field lines. Below 90 km the first term dominates and the ions move with the neutral wind. At altitudes of between 90 and 120 km the second term containing the cross-product motion plays a major role in the movement of the ions.

Theoretical research following this first discussion of the wind shear mechanism for sporadic E formation extended the original theory regarding the ion composition of a sporadic E layer. Axford and Cunnold (1966) considered the effect of multiple ion species being present in a sporadic E layer. They found the maximum electron density in the layer is determined by the ion with the smallest recombination coefficient, even though that ion might be a very minor constituent in the normal E region. This conclusion is strongly supported by rocketsonde results that show the major constituents in sporadic E layers are metallic ions (primarily Mg^+, Fe^+, Si^+) which have very long lifetimes compared to the dominant ions in the E-region, O_2^+ and NO^+. Outside the layers normal E region distributions were present (Young et al., 1967; Narcisi, 1968; Zbinden et al., 1975). Metal ions are presumed to come from meteors.

While the lifetimes for metallic ions are known to be long, little is known about the actual residence times at sporadic E heights. Axford (1963) showed that gravity waves progagating upward could trap ionization at nodes in the neutral wind and move it downward at nearly the phase velocity of the gravity wave. This has been termed the "corkscrew effect," and it is particularly effective in the lower E region. Further work by Chimonas and Axford (1968) showed that the corkscrew

process would periodically sweep metallic ions from the sporadic E region and dump them at the 85-90 km level. Above 95 km the position a sporadic E layer could be predicted using wind shear theory as above; below 95 km such predictions would not be valid because the dumped ions would tend to accumulate at these levels. Some experimental work (Wright et al., 1967; Wright and Fedor, 1969; Rowe, 1974; Miller and Smith, 1978) supports the corkscrew process moving and dumping ionization at lower levels. Whitehead (1971) expanded on the corkscrew effect by showing the spectrum and amplitude of internal gravity waves determine not only the effectiveness of this process but also the direction ionization will move, upward movement being possible with short period waves.

Movement of sporadic E clouds in the horizontal direction is a quantity not often reported in the literature. Whitehead (1971) summarizes the published results on horizontal motion saying it is generally seen moving equatorward at approximately 80 m/s. No definitive answer has been found as to whether this movement is associated with the phase motions of waves moving through the region or whether it is more closely tied to the netural wind motions.

Atomic Oxygen Emissions at 557.7 nm

Atomic oxygen emissions have been studied for many years using sensitive photometer systems. The initial reason for taking these measurements was to calculate atomic oxygen number density profiles. More recently this information has been used to study gravity wave (see Table 1) and tidal wave motions in the middle atmosphere (Petitdidier and Teitelbaum, 1977).

Extensive satellite measurements in the early 1970's confirmed that about 90 percent of the total 557.7 nm emission at mid-latitudes comes from an 8 km-wide layer centered at 97 km (Donahue et al., 1973). This puts the atomic oxygen emission layer at very nearly the same altitude as sporadic E; thus, results from each process can be compared. Some 557.7 emission is also seen from the F region but this is usually quite small.

Two reactions are candidates for generating emissions at this wavelength. The first, suggested by Chapman (1931), is given by:

$$O + O + O \text{ -------- } O_2 + O(^1S) \qquad (2.22)$$

Barth and Hildebrandt (1961) proposed a second, two step process as follows:

$$O(^3P) + O(^3P) + M \text{ ----- } O_2^* + M \qquad (2.23)$$

$$O_2^* + O(^3P) \text{ ----- } O_2 + O(^1S) \qquad (2.24)$$

More recent literature (Slanger and Black, 1977) has tended to support the second of these two reactions.

In any case, the green line emission has been used by several workers (Freund and Jacka, 1979: Meek and Manson, 1983; Battaner and Molina, 1980) to measure gravity wave motions at these heights (Table 1). In each case, these authors have interpreted their observations as phase motions of gravity waves moving through the region.

There is very little literature linking the presence of mid-latitude sporadic E to the intensity of green line emissions even though the two processes occur at very similar altitudes. Whitehead

(1970) reported this in his extensive review on sporadic E as did Petitdidier and Teitelbaum (1977) in their discussion of the atomic oxygen emissions. Here we examine the relationship in a rather basic way by comparing the spectral power densities of the two phenomena. This is further discussed in Chapters III and IV.

CHAPTER III

DATA COLLECTION AND ANALYSIS

Data Collection

The data analyzed in this research were collected at the Boot Lake field site near Brighton, Colorado, and at the Jelm Observatory near Jelm, Wyoming. The primary equipment site was at Boot Lake where the equipment included a medium frequency radar operated as an imaging Doppler interferometer, a NOAA/NSF high frequency radar operated as a digital ionosonde, and a tilting-filter photometer for measuring 557.7 nm emissions from atomic oxygen. At Jelm, all of the equipment was for optical viewing of the sky. Photometers with 1.5° field-of-view (FOV) were available for atomic oxygen intensity measurements.

The Imaging Middle Atmosphere Geophysical Radar (IMAGER) was operated at 2.66 MHz with a 50-kW peak-pulse-power in 30- μs Gaussian pulses. Ten independent coaxial-colinear antennas were used; five parallel in an east-west direction; five parallel in a north-south direction as shown in Figure 6. All ten antennas transmitted simultaneously. For reception, the complex voltages for the antennas were read by pairs in rapid sequence (EW-1, NS-1; EW-2; NS-2; etc.) with the data being recorded on magnetic tape. Transverse antenna spacings of .707λ give grating lobes at $\pm$ 45° to zenith. This means scatterers located within 24.5° of zenith are unambiguous. Outside of this range, scatterers within 45° of horizontal are aliased into zenith angles between 24.5° and 45° on the other side of zenith.

IMAGER (Imaging Middle-Atmosphere Geophysical Radar) ANTENNA

LOCATION: BOOT LAKE (BRIGHTON) COLORADO
AREA: 25.6 ACRES = 10^5 M^2
HEIGHT: 0.15 λ
FREQUENCY: 2.66 MHz
λ: 112.5 M

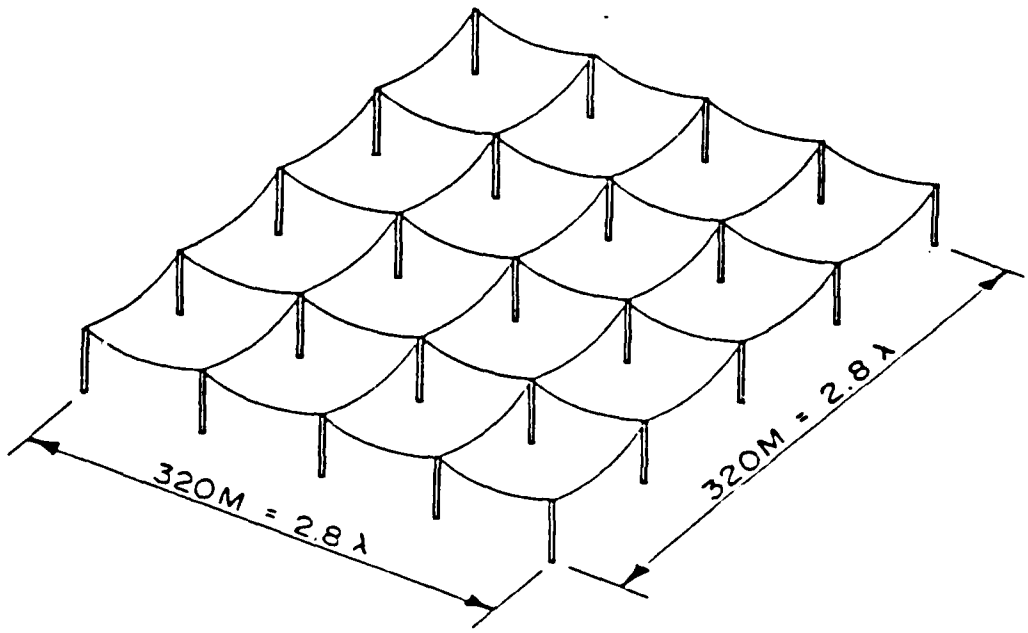

Fig. 6. Antenna array configuration for IMAGER radar (Adams, et al., 1986b).

For the data analyzed here pulses were transmitted every 0.1 s for a period of 12.8 s. A 3-km range-gating scheme was applied to the returned signal. For each pulse, 50 separate range gates were recorded, with the bottom altitude being 58.5 km and the top 208.5 km. Each 128-point set will be referred to as a sounding. Soundings were taken and recorded on magnetic tape every 10 min from approximately 0300-1100 UT on June 25 and 30, 1984. Thus, we have a series of 12.8 s snapshots of the ionosphere for these two nights.

At Boot Lake the ionosonde data were collected using a four-curtain vertex-down log-periodic antenna for transmission and four independent dipoles commuted into two independent receiver channels (Adams et al., 1986a). Once an echo was identified (Grubb, 1979), the quadrature components and virtual height measurements from each antenna were recorded on magnetic tape for postanalysis. With the equipment outlined here, conventional ionogram and echo-location analysis are possible. Here, we consider only the conventional ionogram information.

The ionosonde system was run in two modes, a conventional mode where the frequency was swept from 1.6 MHz to 20 MHz, and a high resolution mode where the frequency was swept between 1.6 MHz and 3 MHz. In both cases, the frequence was swept logarithmically between the end points. Each type of sounding was accomplished every 10 min with data times starting on the hour and 8 min after the hour, respectively.

Photometer data were collected at Boot Lake using a 1.5° FOV tilting-filter photometer as described by Meriwether et al. (1983). The instrument was housed in a NOAA observational trailer and operated through an interface with a DEC LSI-11. Several filters were used for

OH rotational temperature measurements and one filter was available for 557.7 nm green line emissions from atomic oxygen. A 5-point imaging scheme was used with zenith and 25° off-zenith in the four cardinal directions being the positions toward which the instrument was pointed. Total integration time at any one position was 1.5 s for 557.7 nm emissions. Each point was sampled successively every 272 s with data analysis being accomplished while the instrument was rotated to the next position.

The 1.5° FOV photometer at Jelm was fixed in position toward the North Celestial Pole. Measurements of 557.7 nm emissions were taken every 30 s and displayed on a strip chart as well as being digitized and stored on disk for later analysis.

Data Analysis

The analysis of radar interferometry data outlined below follows closely the procedures developed by Adams et al. (1986b).

Interferometry makes use of the phase difference between received signals at two or more spatial locations. High speed electronic equipment makes it possible to measure phase differences in received voltages for radio frequencies typically used by atmospheric radars (2-1000 MHz). To illustrate interferometry techniques consider the gain pattern from a dipole antenna above a ground screen (Figure 7a). If we wish to control this gain pattern a second antenna can be added as shown in Figure 7b. Here, the antennas are spaced $\lambda/2$ apart and are transmitting in phase. By introducing a phase shift between the two antennas the transmitted beam can be steered as shown in Figure 7c. The relationship between the phase shift ϕ and the steering angle θ is given by:

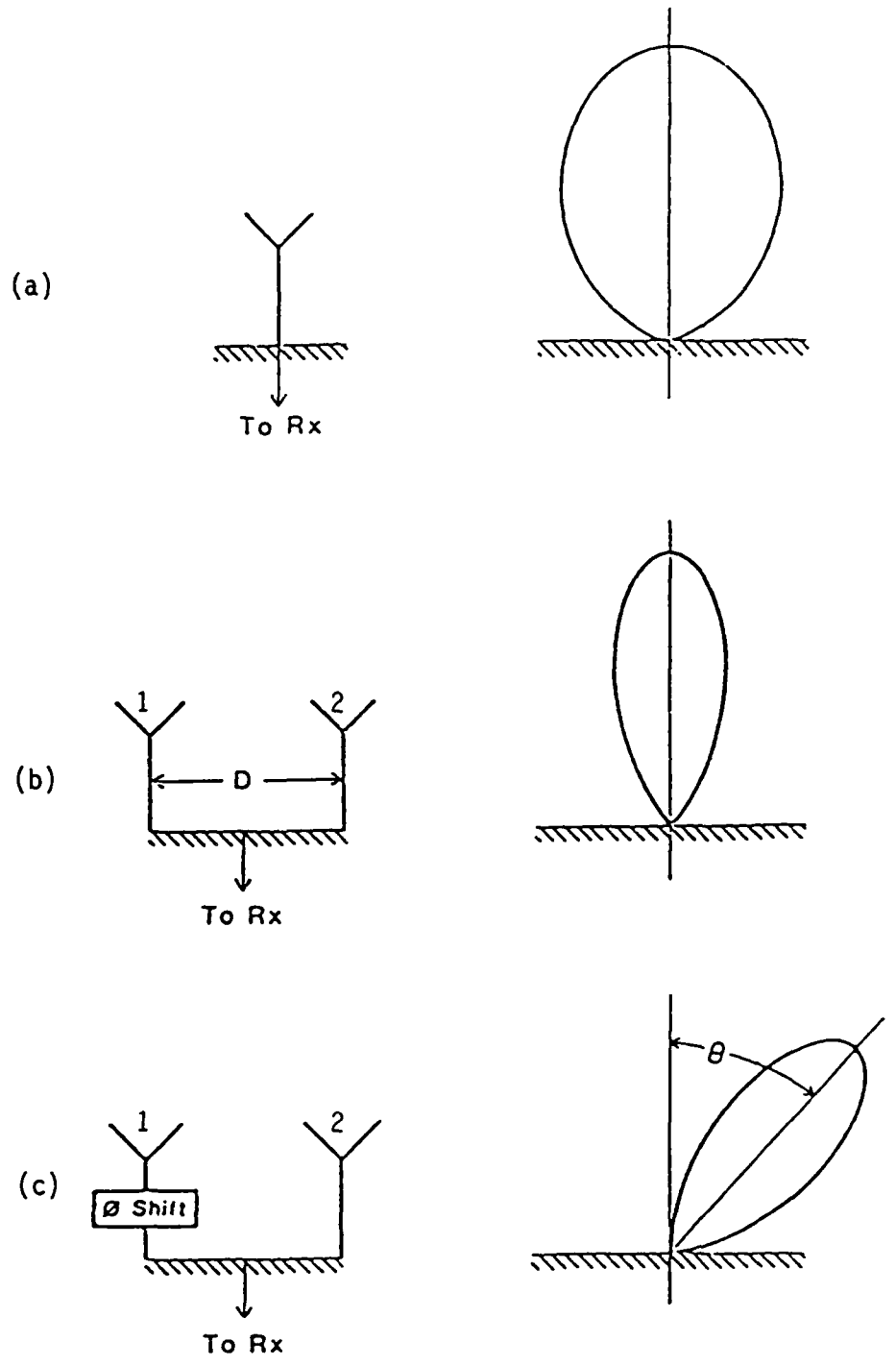

Fig. 7. Schematic diagram illustrating gain pattern for (a) Single dipole antenna, (b) A pair of dipoles connected in-phase, and (c) Pair of dipoles connected with phase shift in one leg (Adams, et al., 1986b).

$$\phi_2 - \phi_1 = \frac{-2\pi D \sin\theta}{\lambda} \qquad (3.1)$$

where D is the distance between the two antennas.

The above approach can be used for the received signal if the complex voltages from each antenna are measured independently. In this case a mathematical rather than a physical antenna beam can be formed. For a vertically directed beam the two complex voltages are simply added together at each instant giving:

$$V_s\ (\theta = 0, t) = V_1\ (t) + V_2(t) \qquad (3.2)$$

If the beam is steered to some angle θ_s the required phase shift is calculated from equation 3.1 and the steered voltage is given by

$$V_s\ (\theta = \theta_s, t) = V_1\ (t)\ e^{i\phi_s} + V_2(t) \qquad (3.3)$$

The returned signal, if we consider it to be a sum of signals from discrete scattering points, exhibits very complex temporal variation. A Fourier transform of this time domain record makes it possible to identify these individual scattering points. In the frequency domain each scattering point can be separated by frequency as long as the radial velocities are distinct.

To illustrate this approach, consider the case of a single scattering point moving horizontally at velocity V_h (Figure 8). Fourier transform of the time series complex voltages from each antenna provides power and phase spectra as shown in Figure 9. Both power spectra identify the same Doppler frequency f_t, which can be used in equation 3.4 to get the radial velocity V_r:

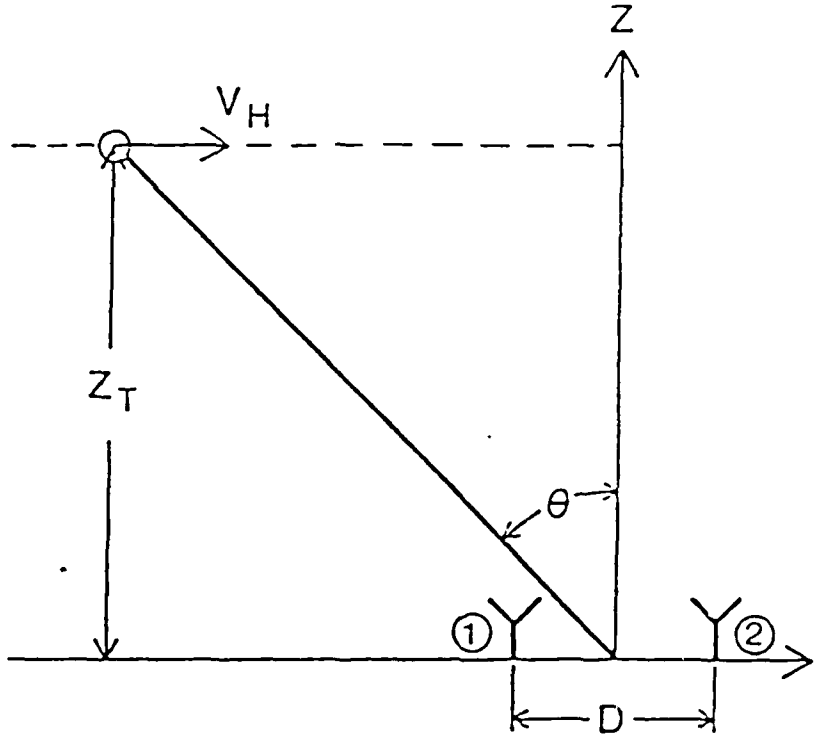

Fig. 8. Geometry for a single horizontally moving target being observed by a two-antenna interferometer (Adams, et al., 1986b).

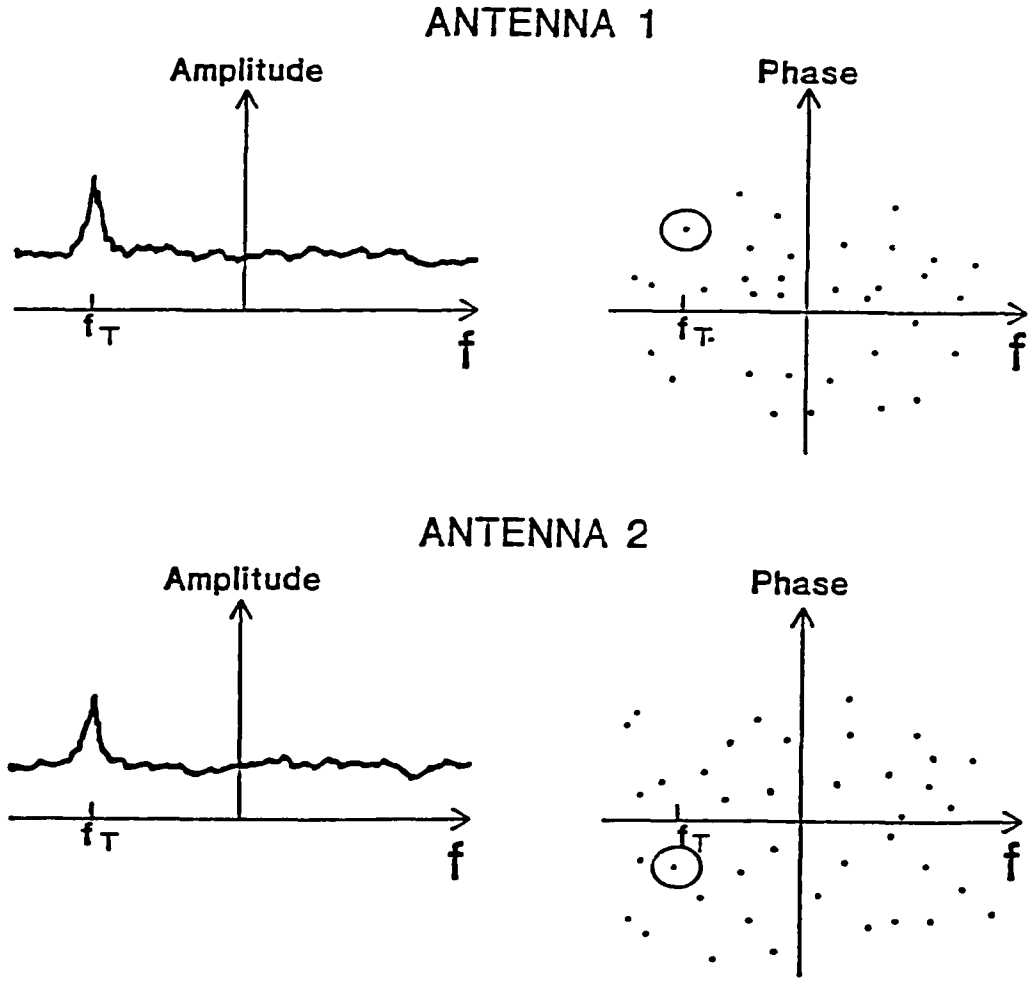

Fig. 9. Complex Fourier spectra for the two antennas in Figure 8, showing the signature of a single moving target (Adams, et al., 1986b).

$$V_r = \frac{f_t c}{2F} = V_h \sin\theta \qquad (3.4)$$

where f_t is the Doppler frequency, F is the radar frequency and c is the speed of light. The difference in phase values at f_t can be used in equation 3.1 to calculate the zenith angle of the target, θ_t. This transform process is not particularly useful for a single scattering point since phase differences could be studied directly in this case. The advantage of Fourier transform becomes evident when considering multiple scattering points.

Figure 9 might seem to indicate the criterion for defining a scattering point is large amplitude at a given frequency on both antennas. This is not the case. The multiplicity of antennas in this experiment makes it possible to use the root-mean-square (rms) error of a least squares fit line of phase versus ground distance (or antenna number since distance between antennas are the same) as the condition for determining whether a scattering point is real. Before this was done each phase value had to first be corrected for the time lag introduced in commuting 10 antennas into two receivers and then for 2π discontinuities (Adams et al., 1985). This was done on both the N-S and the E-W antenna sets independently. A point was accepted as real if the sum of the rms error from each set of antennas was less than 40°. Modeling calculations show that about one noise point per 128 point data set was accepted when we used this criterion (Adams et al., 1986b). Once a valid target is identified in this manner, the mean slopes of fitted lines can be used in equation 3.1 to calculate the zenith angle in the appropriate plane.

Consider the information we have available about each scattering point:

f - the Doppler frequency, which gives the radial velocity from equation (3.4);

R - range gate, in 3 km steps increments;

θ_{EW} - echo location angle in the E-W plane;

θ_{NS} - echo location angle in the N-S plane.

Now R, θ_{EW}, and θ_{NS} form a three-dimensional coordinate system that can be transformed into a Cartesian coordinate system where x is east, y is north, z is vertical. From the echo location angles the altitude of each point can be calculated using equation 3.4.

At this point of the analysis we applied a gridding scheme to the scattering point data (G. Adams, private communication, 1986) rather than using the individual points. The entire 24° X 24° viewing area was divided into 1° X 1° squares. Within each square, a power weighted average Doppler frequency was calculated and assigned to the center of that square. This scheme was applied very successfully at low levels (Coble, 1987) where highly aspect sensitive returns limit the spatial extent of the viewing area. We used it in a region where aspect sensitivity is not generally a problem for two other reasons. First, gridding gives a better representation of the mean velocity at a given altitude by eliminating clusters of points that would otherwise unduly influence the results if all the points were considered individually. By giving more weight to stronger returns we are in effect saying the stronger a point the more likely it is a real point rather than simply noise slipping through the selection process.

Having determined the location of each mean scattering point, velocity calculations are possible if there are enough scattering points at a given altitude (a minimum of three points for horizontal and vertical components, two if only horizontal winds are considered). The vector radial velocity is given by

$$\tilde{V}_{Rj} = V_{Rj}\tilde{1}_{Rj} \tag{3.5}$$

where $\tilde{1}_{Rj}$ is a unit vector in the radial direction passing through the jth point at a given altitude. It is given by

$$\tilde{1}_{Rj} = 1_j\tilde{1}_x + m_j\tilde{1}_y + n_j\tilde{1}_z \tag{3.6}$$

Here, 1_j, m_jk and n_j are the direction cosines of the jth scattering point given by

$$1 = \sin\ \theta_{EW} \tag{3.7}$$

$$m = \sin\ \theta_{NS} \tag{3.8}$$

$$n = (1 - 1^2 - m^2)^{\frac{1}{2}} \tag{3.9}$$

The mean apparent motion vector is then given by

$$\tilde{V}_m = u\tilde{1}_x + v\tilde{1}_y + w\tilde{1}_z \tag{3.10}$$

where u, v, and w are the components of velocity in the east-west, north-south, and vertical directions, respectively.

With more than three points a least squares fit to the scattering point can be calculated. Since

$$V_{Rj} = \tilde{V}_m \cdot \tilde{1}_{Rj} \tag{3.11}$$

for all j if the rms fit is perfect, the rms error is given by

$$\epsilon = (1/J \sum [V_{Rj} - (ul_j + vm_j + wn_j)]^2)^{\frac{1}{2}} \qquad (3.12)$$

The choices of u, v, and w that minimize require

$$\frac{\partial \epsilon}{\partial u} = \frac{\partial \epsilon}{\partial v} = \frac{\partial \epsilon}{\partial w} = 0 \qquad (3.13)$$

which gives

$$u \sum l_j^2 + v \sum l_j m_j + w \sum l_j n_j = \sum V_{Rj} l_j \qquad (3.14)$$

$$u \sum l_j m_j + v \sum m_j^2 + w \sum m_j n_j = \sum V_{Rj} m_j \qquad (3.15)$$

$$u \sum l_j m_j + v \sum m_j n_j + w \sum n_j^2 = \sum V_{Rj} n_j \qquad (3.16)$$

The mean velocities in the x, y, and z directions are then calculated at each altitude by solving equations 3.14-3.16 simultaneously.

Photometer data analysis as used in this research is relatively straightforward. As was outlined in the previous section, the 557.7 nm intensity information at Boot Lake was available from five different directions. From this data, we were able to calculate "correlation velocities" by simply comparing the time series records from each of these different directions. Correlation velocities obtained here are then compared to velocities obtained with the Doppler interferometer.

We also used a simple Fourier transform routine to calculate spectral power densities for the 557.7 nm atomic oxygen line data from June 30, 1984. These are then compared to similar curves of received power from the radar system.

CHAPTER IV

RESULTS AND DISCUSSION

Traveling Ionospheric Disturbances

The Doppler interferometer system described earlier is the primary source for the results discussed here. Two nights of data collection are considered: 0208-1058 UT, June 25, 1984 (1908-0358 MST, June 24-25, 1984) and 0318-1058 UT, June 30, 1984 (2018-0358 MST, June 29-30, 1984). From this point on we will refer to these days by their Julian calender numbers, days 177 and 182, respectively. Only on these two nights, when there was sufficient ionization present in the lower E region, were we able to get enough scattering points to allow us to examine velocities at these heights.

This is in fact our first observation - when running in the rapid scan mode (i.e. no coherent averaging done) the radar was not able to get enough points to determine velocities unless there was a sporadic E layer present (further discussion of sporadic E will follow in the next section). It was present for much of the period of day 182 so a fairly complete data record is avaiiable. On day 177 there was only a two hour period between 0738-0928 UT where this was the case.

On day 182 the mean velocities were consistently between 200 and 325 m/s at all altitudes between 88 and 109 km. Not only were the velocities relatively constant in magnitude with height, the directions were consistently toward the south and west through this same layer. These results are shown in Figures 10 and 11, respectively. In both

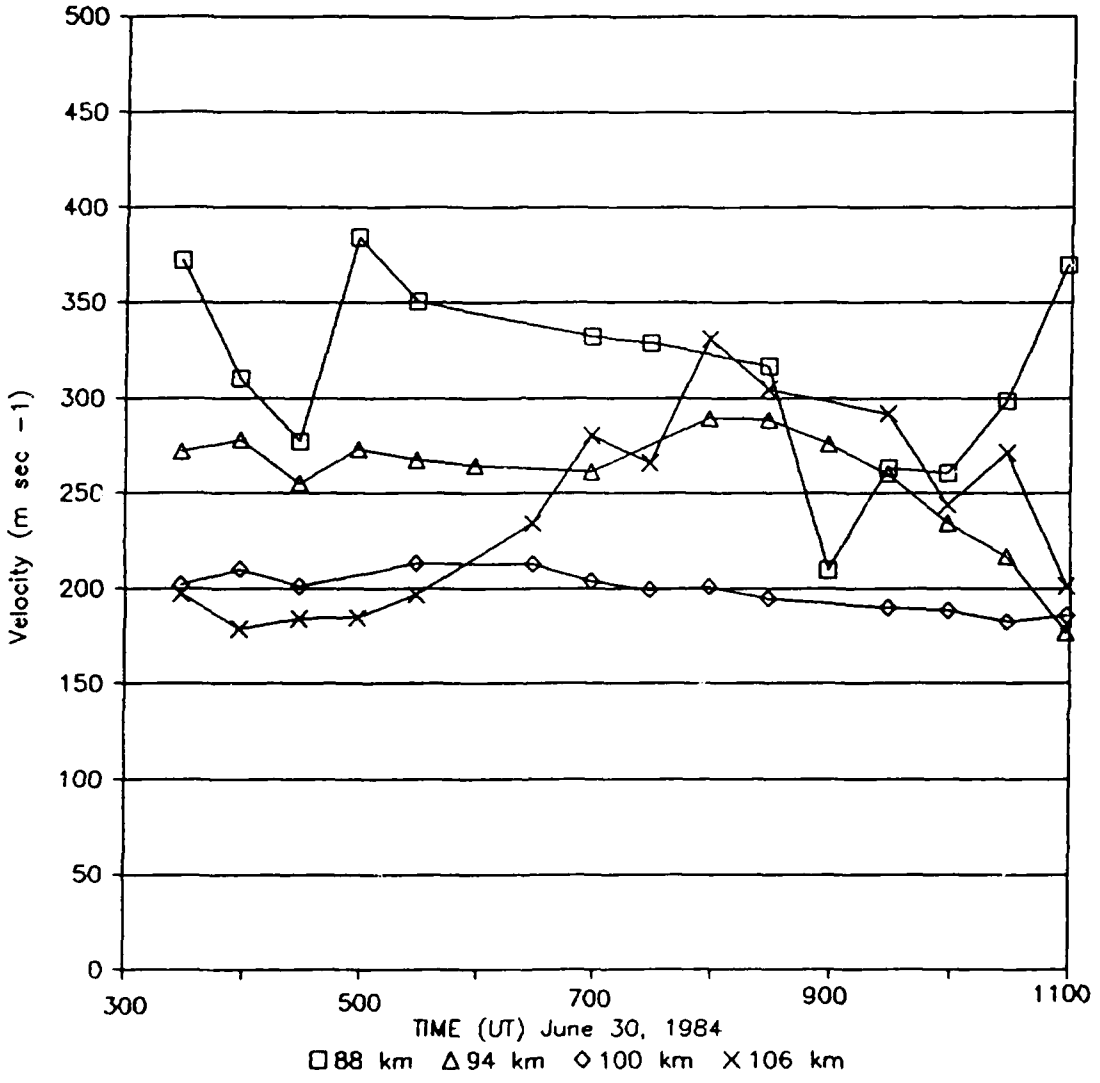

Fig. 10. Magnitudes of horizontal velocity vectors at 88, 94, 100, and 106 km for Day 182.

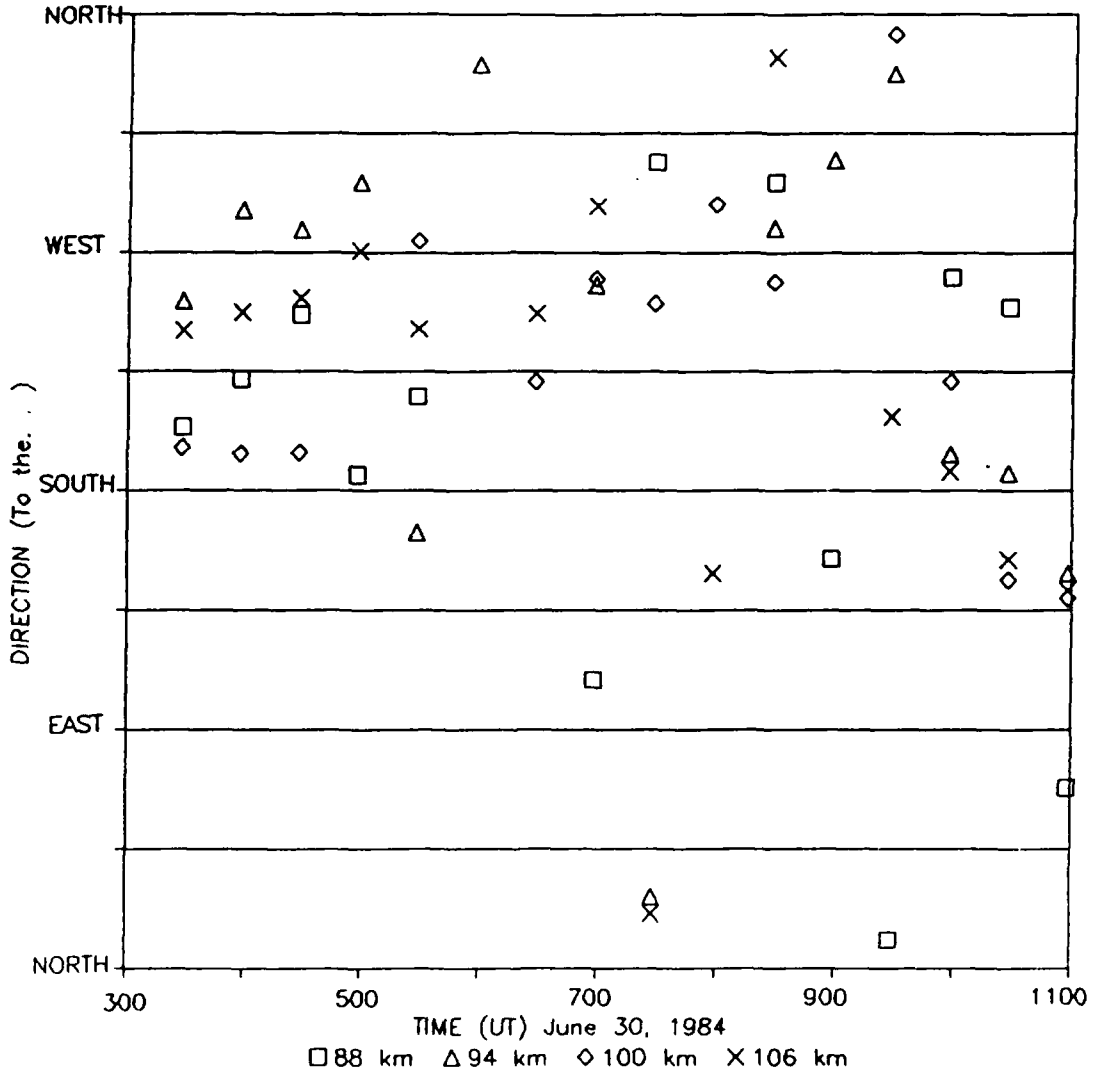

Fig. 11. Directions of horizontal velocity vectors at 88, 94, 100, and 106 km for Day 182.

figures we have combined soundings in groups of three (i.e. 30-min averages) so that we could get enough scattering points at each of these altitudes to make these velocity calculations. After eliminating all soundings with 2.25 times the standard deviation of the velocities from each sounding, we also 5-point smoothed the results. The figure of 2.25 times the rms error was arrived at through trial and error. If these velocities were normally distributed, this value means we would be accepting 88 percent of all points going into the average.

In Figures 12 and 13, we have singled out the 100 km level from day 182 as representative of all the curves shown in Figures 10 and 11. In a similar fashion, the results for the 106 km level on day 177 are shown in Figures 14 and 15. We were able to plot individual soundings in each of these four figures because there were enough points available to do so.

We interpret these results as evidence that medium scale TIDs are present and moving through the E region with the speed of propagation being the phase velocity of the internal gravity waves. This interpretation fits very well with Georges medium scale TID propagation speed in the F region of between 100 and 300 m/s. The equatorward direction of travel also is in general agreement with many past observations.

It is difficult to interpret these results as very strong background and/or pertrubation winds that we simply happened to observe for two nights. Many previous observations of bulk velocities at these heights (Bedinger et al., 1968; Rosenberg, 1968; Meek and Manson, 1983) show that such motions rarely exceed 100 m/s. Riggin et al. (1986) reported observing motions exceeding 200 m/s in a mid-latitude sporadic E layer. However, these were gravity wave induced perturbation

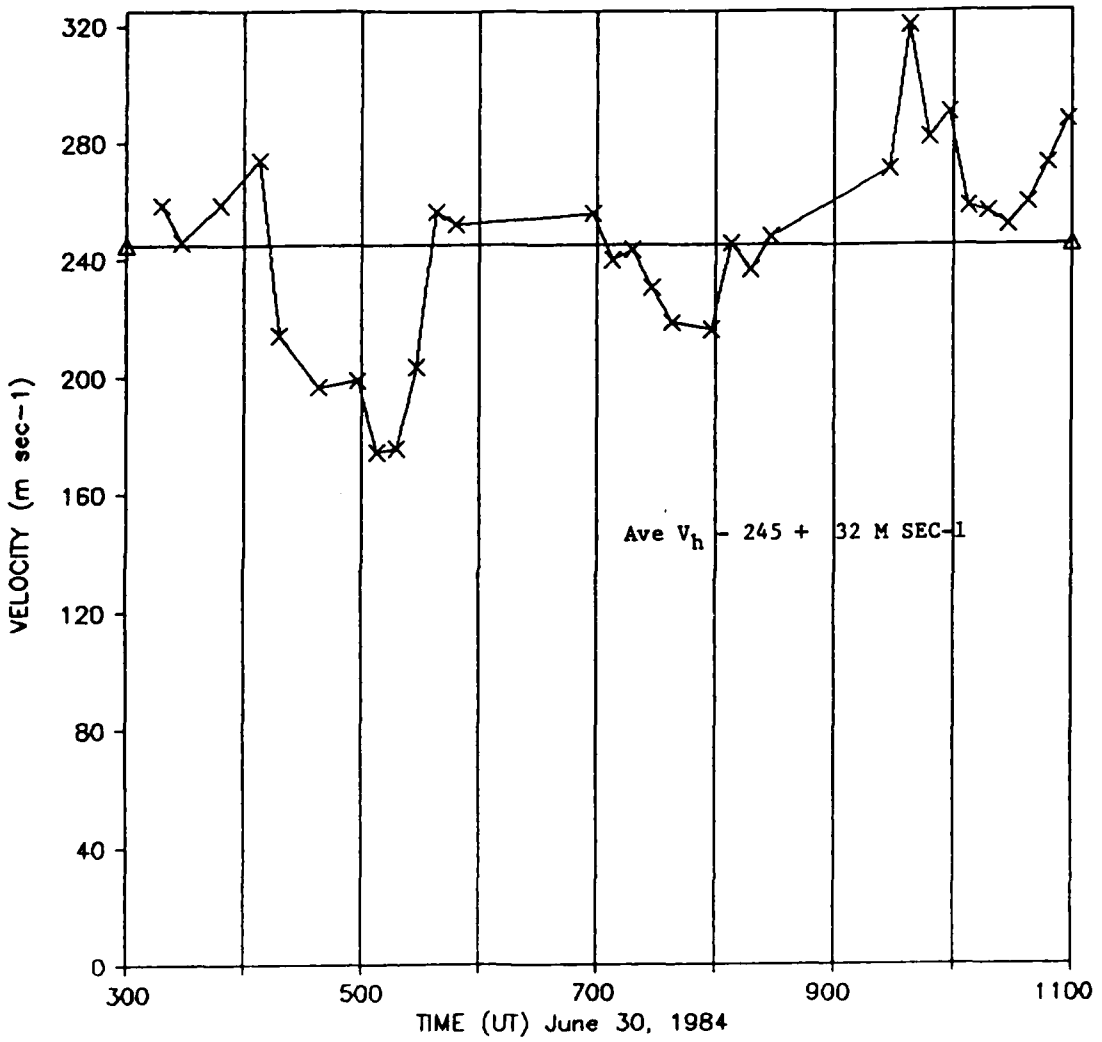

Fig. 12. Magnitude of horizontal velocity vectors for 100 km on Day 182.

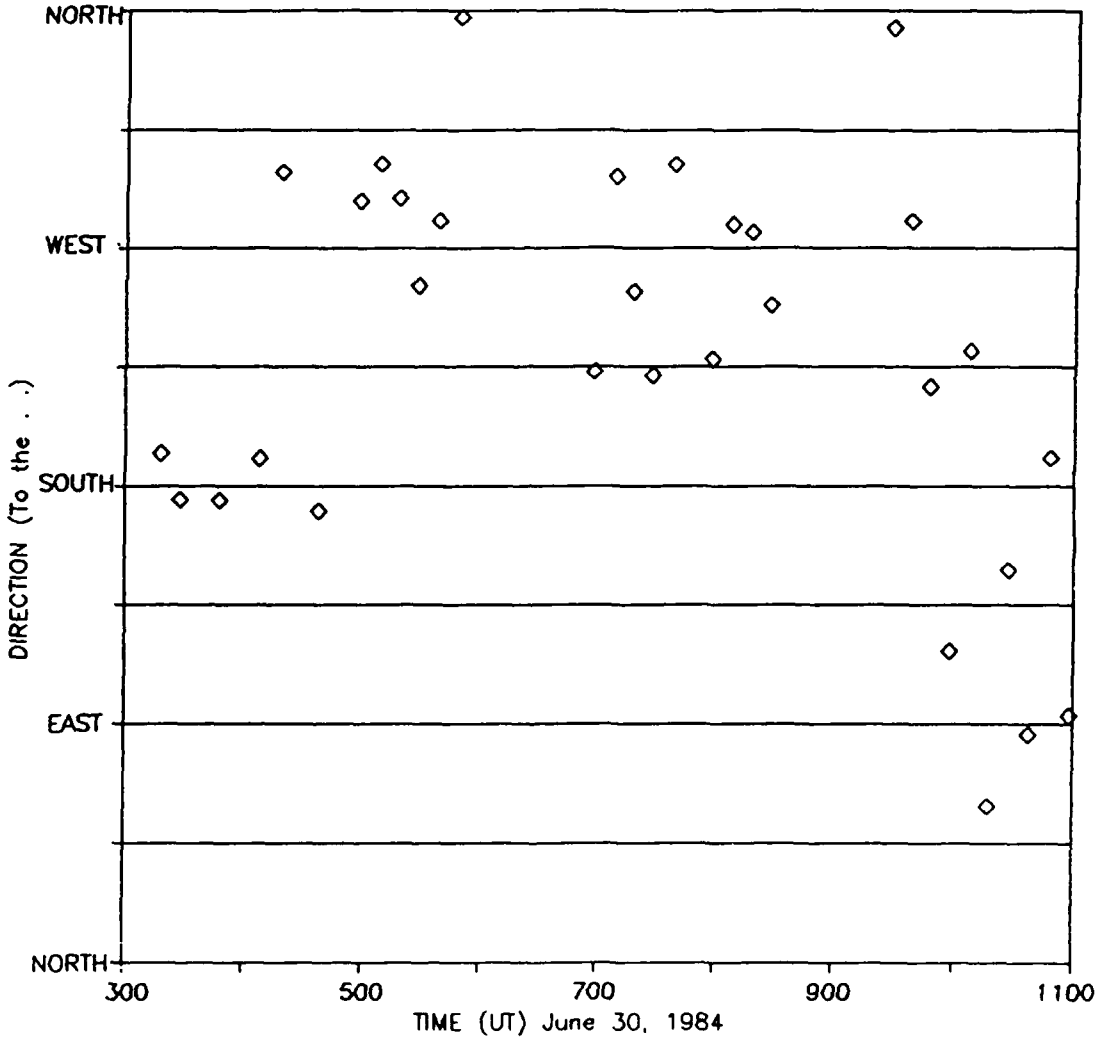

Fig. 13. Direction of horizontal velocity vectors for 100 km on Day 182.

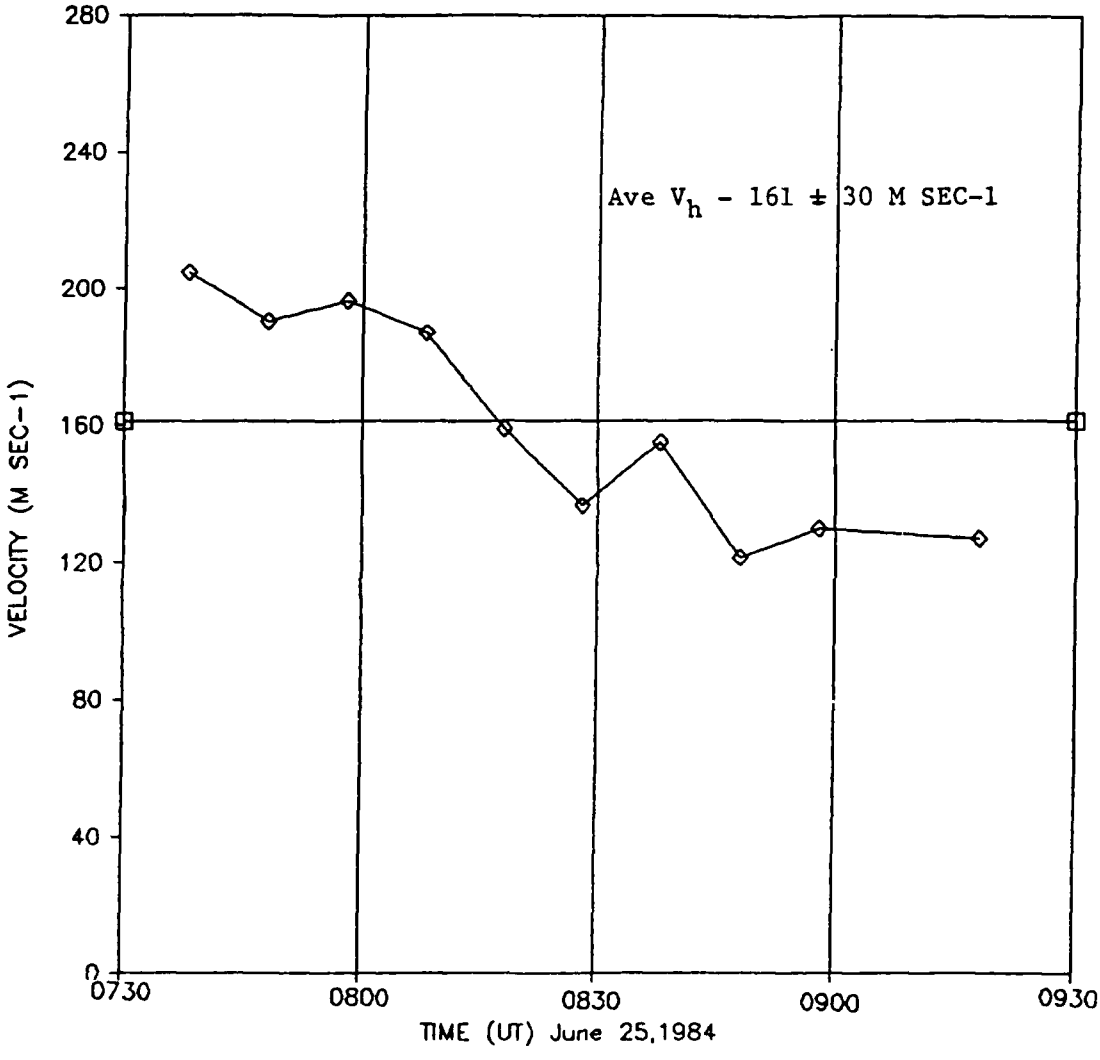

Fig. 14. Magnitude of horizontal velocity vectors for 106 km on Day 177.

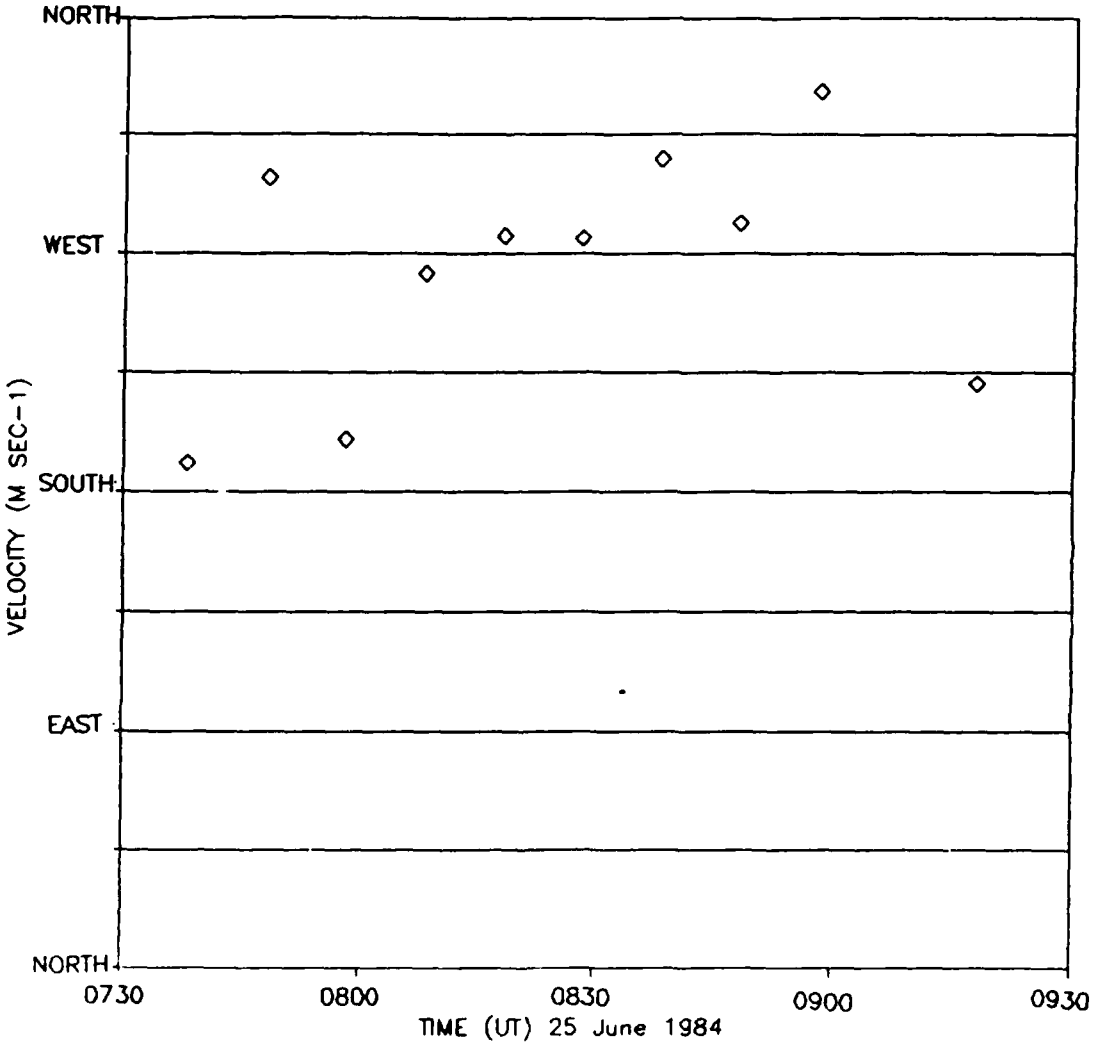

Fig. 15. Direction of horizontal velocity vectors for 106 km on Day 177.

velocities that reversed direction on a time scale of minutes. Our results show consistent direction and speed over a period of 8 hours.

Our results are also constant with height through a 20 km thick layer. This is not characteristic of neutral wind motions in the lower thermosphere which have a vertical wavelength of approximately 20 km (Rosenberg, 1968).

The above discussion tends to eliminate bulk motions as the source of these apparent-velocities. Even so we must ask ourselves, "Is there something in the analysis process has biased our results upward into this range of velocities? We were unsuccessful in our attempts to find such a problem as we discuss below.

Others have obtained quite reasonable wind values at lower altitudes using the same radar system described earlier (Adams et al., 1986b; Turek, 1986; Coble, 1987). Our mode of operation was different than in those cases. Here, there was no coherent averaging of the returned signal and there were only 128 pulses per pulse set instead of 256 or greater. Could these differences explain the large velocities found here?

First of all, we consider the effect of coherently averaging the returned pulses. Coherent averaging effectively reduces the maximum resolvable frequency by a factor of n where n is the number of pulses coherently averaged. Here, by design, no coherent averaging was done, giving us a large frequency spectrum to work with. This, in turn, gives us a large horizontal velocity spectrum (see equation 3.4) that includes high speed motions not seen when coherent averaging is employed. By itself, a short pulse-to-pulse timing interval simply gives a large maximum velocity.

Next we consider the effect of the data record length. Because of hardware limitations and a strict data collection schedule the length of each data record was only 12.8 s. In the frequency domain this short data record means we get only a coarse look at the broad frequency spectrum we obtained by using the short pulse-to-pulse timing. We used the conservative nature of the Fourier transform to estimate the effect this might have on the measured velocities. By shifting every frequency to the next smaller bin and recalculating the velocity and repeating the procedure after shifting the frequencies to the next larger bin we obtained error bound of sorts on the calculated velocity. This error was only on the order of ± 20 m/s, with the lower value being the one of importance here. This still does not put the measured velocities in a reasonable range to be considered bulk wind motions even if we could explain the similar direction through a 20 km deep layer.

At this point it is interesting to note that results similar to ours were obtained on another occasion for the same altitude region when four-pulse coherent averaging and a long data record (410 s) were used (G. Adams, private communication, 1987).

It is clear the mode of operation governs the extent of the velocity spectrum and the minimum number of discrete frequencies available to investigate that spectrum. But in this instance it is the data, not any limitations imposed by the radar, that give us the results we report here.

The Fourier transform process itself might contribute to higher velocities if there were large peaks in the time domain record. These peaks would also be present in the frequency domain along with several harmonics. If these harmonics slipped through the scattering point

selection process they would generate phantom points at high frequencies which could translate to correspondingly high velocities. The Fourier transform is the best place to see if this type of problem is occurring. If it were, we would expect to see a large peak in the low frequency range with several large amplitude harmonics at higher frequencies. Figure 16 is the Fourier transform of the 0318 UT sounding from day 182. It has the largest peak near the central frequency of any sounding in the entire data set and yet there is no evidence that harmonics are a problem.

The altitudes of interest in this research coincide with the meteor height range. Could these in some way be affecting the results we report here? If we assume meteors are sporadic in nature, they would produce a relatively constant number of scattering points throughout the observation period (Davies, 1966). This was not the case. For example, on day 177 the radar ran for nearly five hours without getting enough points at any altitude for a velocity calculation. We therefore discount meteors as a significant source for scattering points in this data set and conclude they have little effect on the results seen here.

We have interpreted the velocities observed as the phase motions of internal gravity waves moving through the lower thermosphere. The nearly constant direction and velocity suggest steady sources located to the north and east of Boot Lake. Southward directed phase velocities suggest an auroral zone source as many previous authors have pointed out (see Table 1). The Kp indices during our observation period were all low (between 2 and 3) indicating relatively quiet geomagnetic conditions. While it is possible that even weak auroral activity could continuously generate internal gravity waves propagating southward,

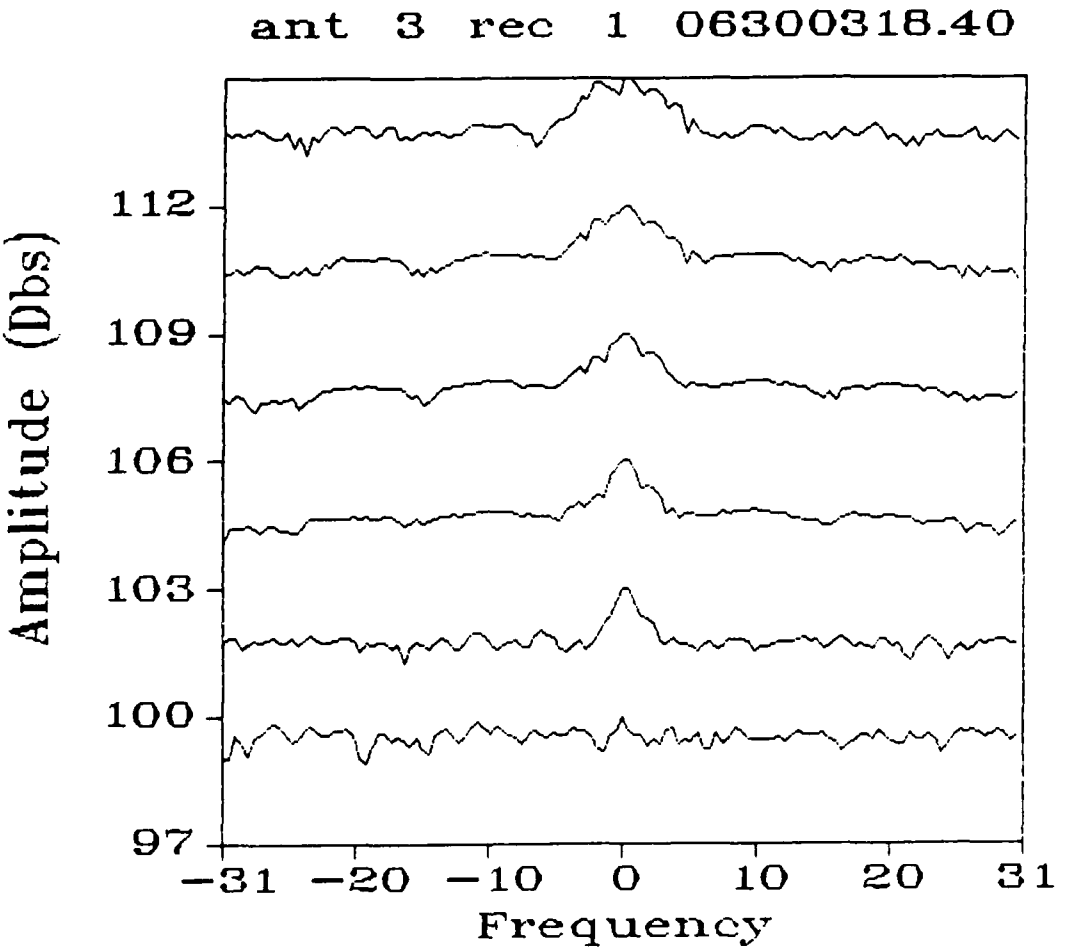

Fig. 16. Fourier transform of 0318 UT sounding from Day 182 showing no strong harmonics are present that could affect the resulting velocity.

this activity can't explain the large zonal component we also see for much of the night.

As was discussed in the Literature Review, tidal motions breaking in the lower thermosphere have been proposed as a continuous source for gravity waves. If this were the case these waves would show the clockwise diurnal tide variation over time (Waldock and Jones, 1986). Our data show at best an oscillatory motion with no trend in the clockwise direction. We can eliminate this source as the primary one driving the apparent-motions we see with the IMAGER system.

Weather phenomena in the troposphere have long been suspected of generating gravity waves that propagate upward into the E region. Figures 17-19 depict the tropospheric weather situation on day 1982. Figures 17 and 18 are radar charts for 0335 UT and 1035 UT, June 30, 1984, respectively. These times were chosen to bracket the times the IMAGER was in operation. Figure 19 is the 0000 UT, June 30, 1984, 300 mb chart. The 300 mb shows a large ridge of high pressure centered over the north-central United States and oriented in a southwest to northeast direction. As might be expected with a ridge in this position there is no precipitation of any type to the north and east of Boot Lake, so thunderstorms can be eliminated as a source for gravity wave phase motions from the east.

Because of the position of the high pressure ridge, we can also eliminate mountain lee waves as a source for gravity waves moving through this region. The generation of these waves requires strong wind flow perpendicular to the orientation of the mountain chain. In this case we have weak flow ($\sim$ 20 m/s) paralleling the mountains. Even if lee waves were a point source for internal gravity waves we

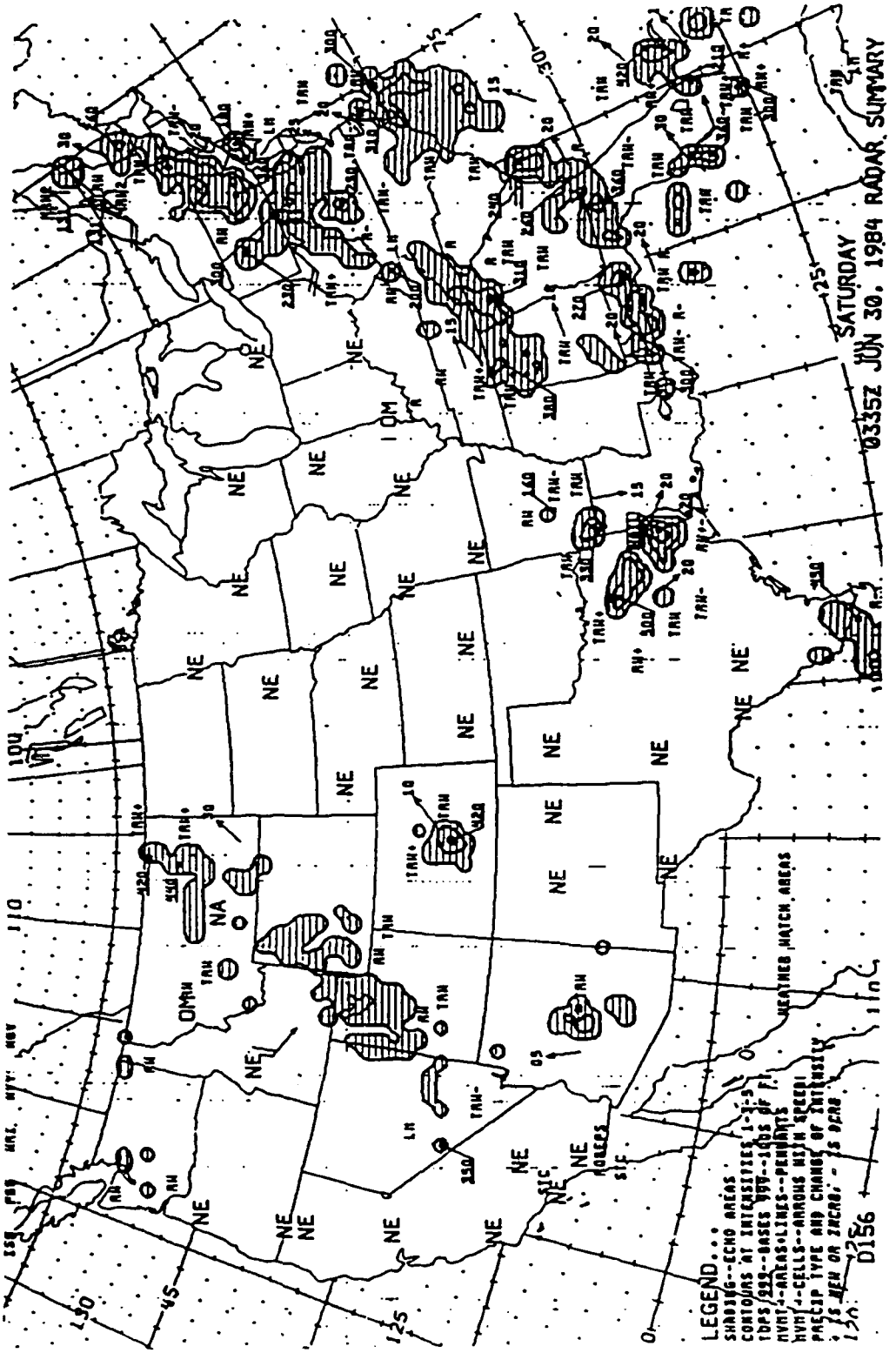

Fig. 17. Radar chart for 0335 UT June 30, 1984 (Day 182).

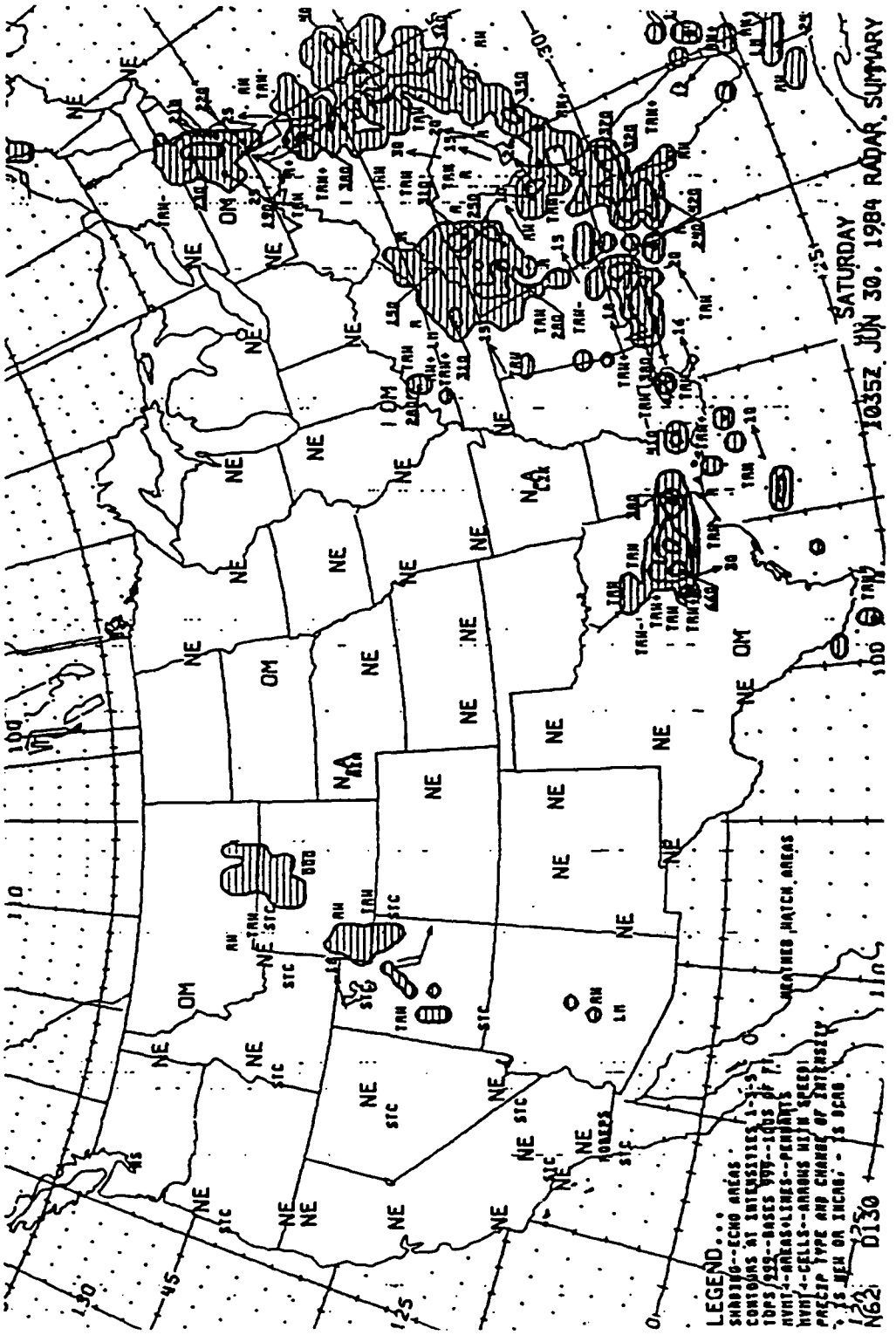

Fig. 18. Radar chart for 1035 UT June 30, 1984 (Day 182).

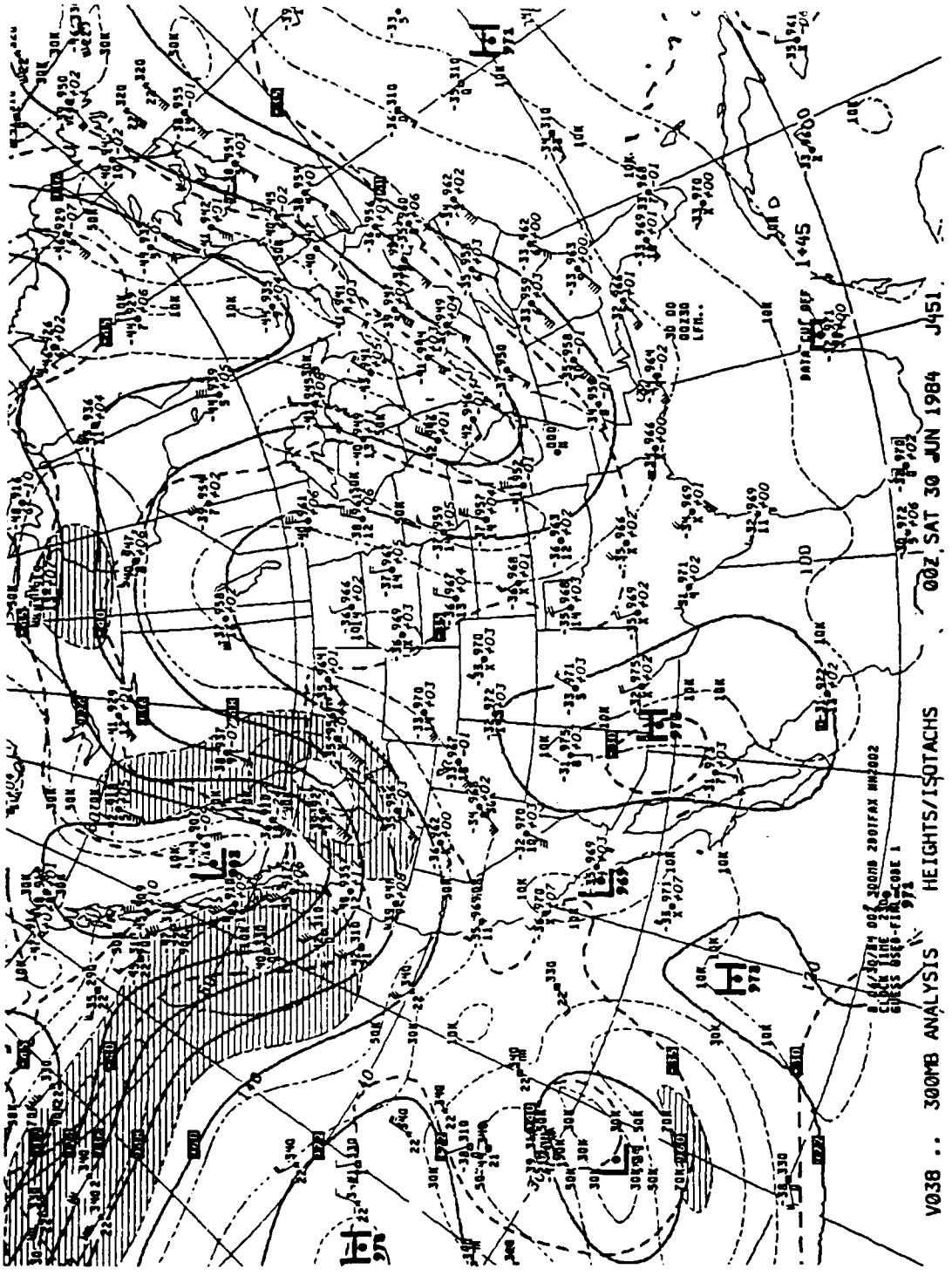

Fig. 19. 300 mb chart for 0000 UT June 30, 1984.

would likely see only north-south motions because of the direction of gravity wave propagation in the vertical (Hines, 1974b).

Low pressure systems to the east and northwest of Boot Lake offer the most reasonable source regions for the gravity wave motions we see on day 182. Although the upper air flow around the eastern trough is not very strong at 300 mb (70 kts or 35 m/s over eastern Kansas), the point of maximum curvature in the flow is almost directly east of Boot Lake. For a good portion of night (approximately 0430-0830 UT) the motions we measured were almost directly from this azimuth. We note that after about 0830 UT the direction transitioned counterclockwise from the east to the northwest by 1020 UT. It is possible the motions over Boot Lake were dominated by the eastern trough for much of the night but as both systems moved east the western trough eventually became the dominate system. It is unfortunate that measurements were not continued beyond 1058 UT to see if this direction held until the western trough passed over Boot Lake.

Although the data record on day 177 is much shorter we can do a similar analysis for the motions seen here. Figures 20-22 illustrate the pertinent tropospheric weather during this period. Figures 20 and 21 are radar charts from 0735 and 1035 UT on June 25, 1984, respectively, and Figure 22 is the 1200 UT June 25, 1984, 300 mb chart which is closest to the IMAGER observation time. Here we notice a large cluster of thunderstorms located over central Nebraska. These thunderstorms remained at the same azimuth from Boot Lake between 0700-0930 UT; it is interesting to note the direction of motion measured by the IMAGER also remained nearly constant from this same azimuth during this time period. After 0930 UT the thunderstorms dissipated rapidly which would mean that

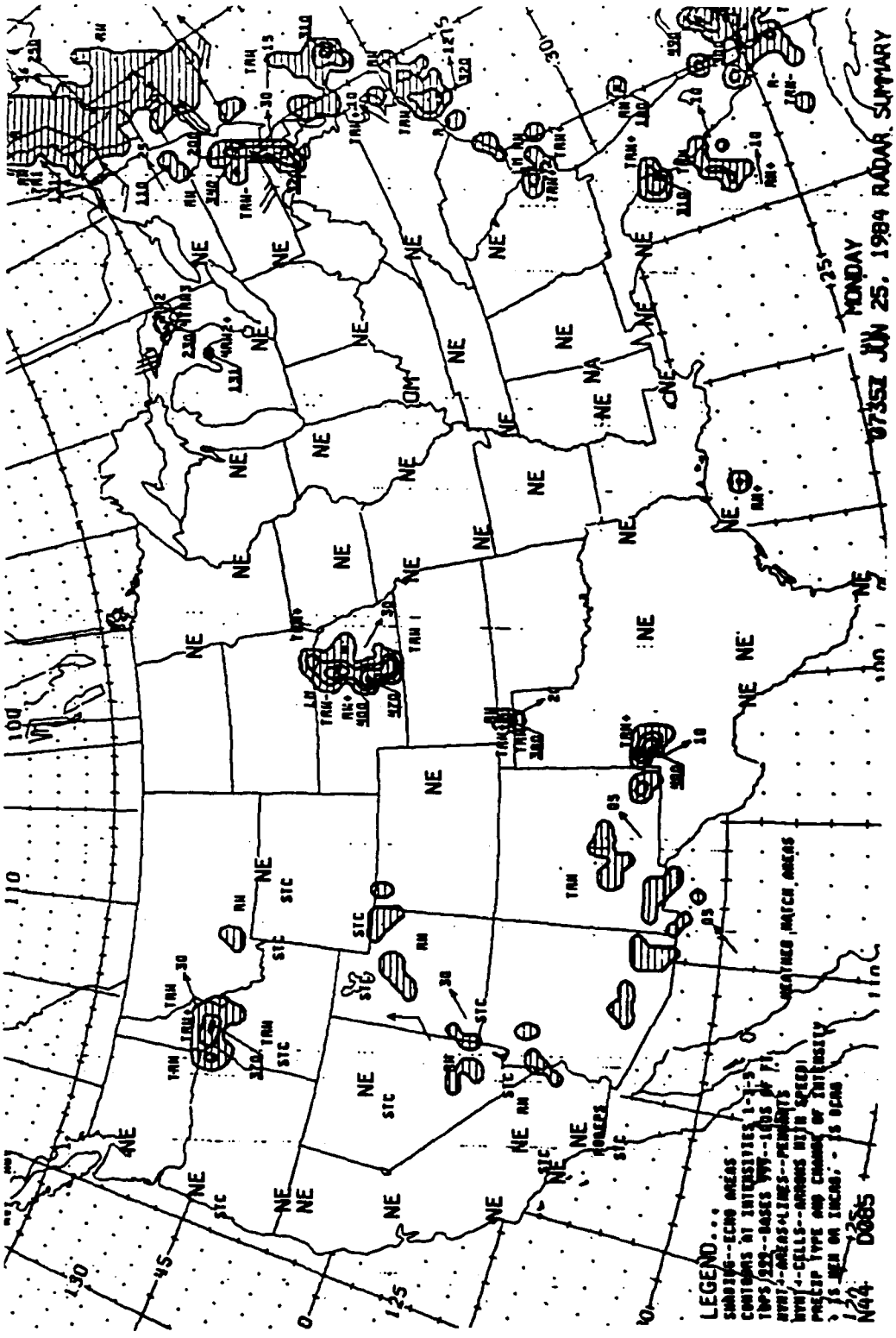

Fig. 20. Radar chart for 0735 UT June 25, 1984 (Day 177).

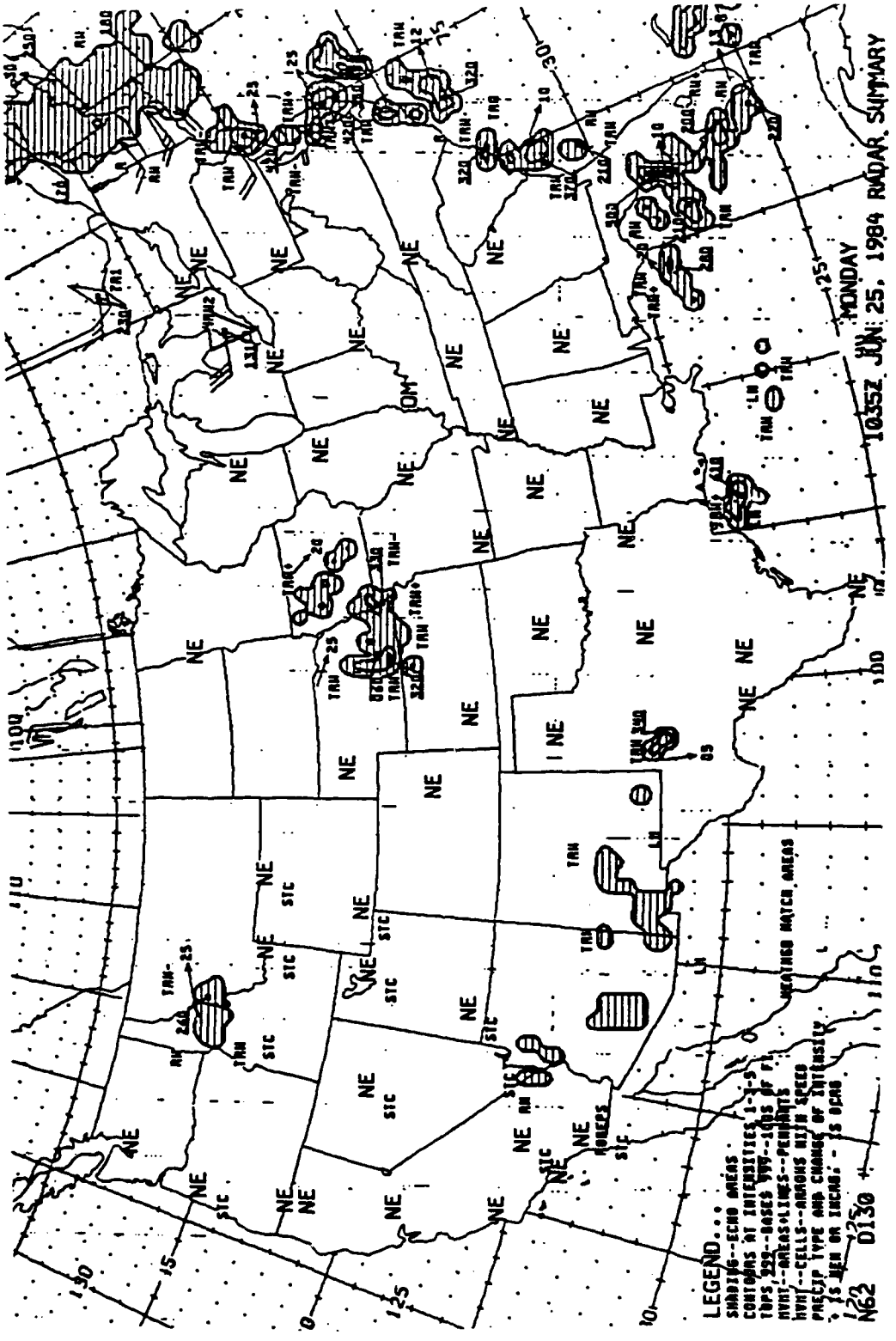

Fig. 21. Radar chart for 1035 UT June 25, 1984 (Day 177).

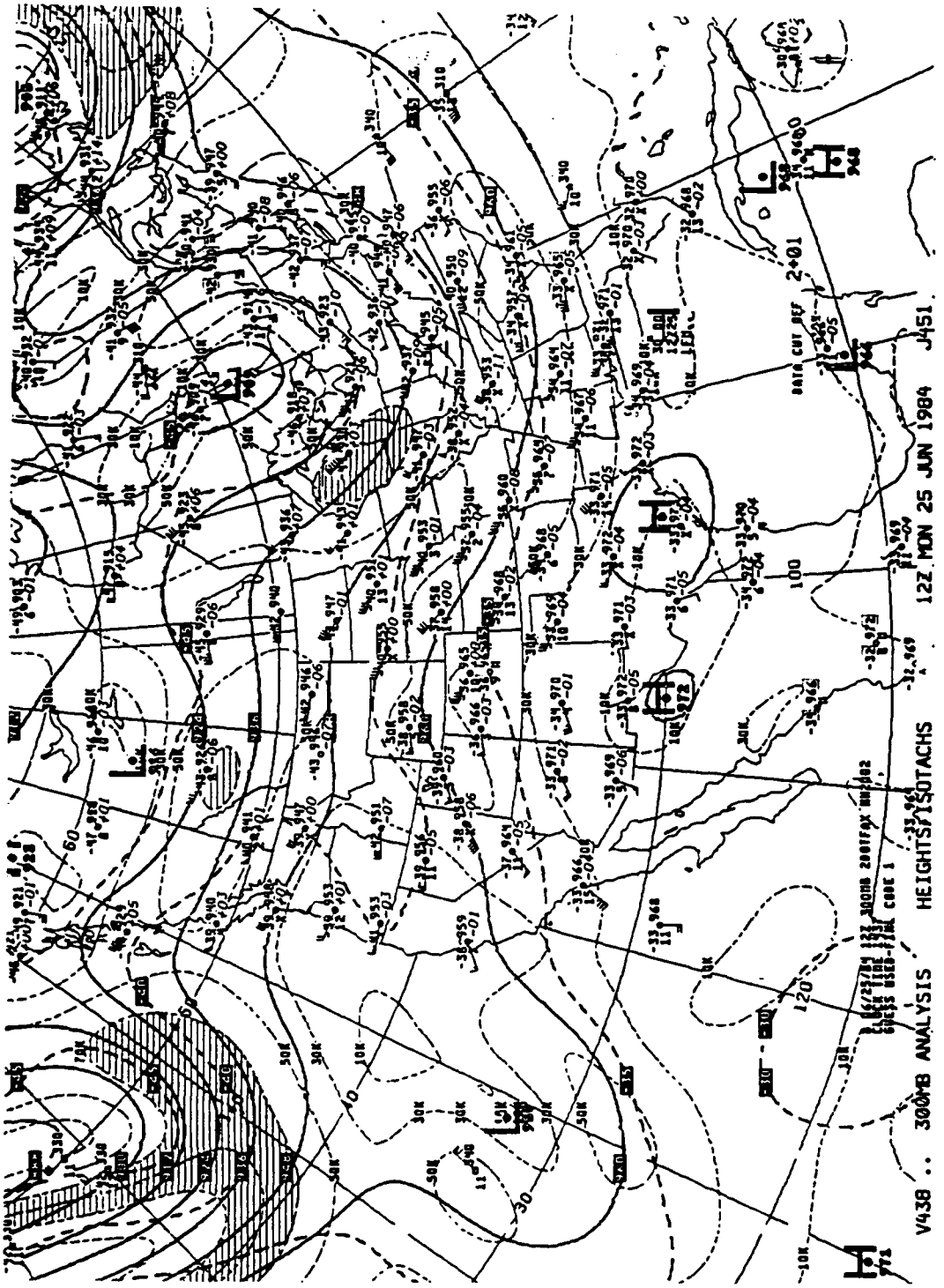

Fig. 22. 300 mb chart for 1200 UT June 25, 1984 (Day 177).

other sources could dominate the motions seen by the radar. The direction of motion seen on the IMAGER swung toward the south at about this same time.

The upper level wind flow on day 177 is much more zonal than it was on day 182. The generation of gravity waves from a single source region is much less likely here because of the weak flow and lack of curvature found in the wind field.

Auroral sources can again be eliminated as the magnetic indexes were rather low. The data record is too short to consider the effects of tidal motions.

Despite our arguments in favor of phase motions of gravity waves moving through the region almost identical findings by G. Adams (private communication, 1987) using another data IMAGER data set, C. Philbrick (private communication, 1987) using a lidar system in the auroral zone, and Kelder and Spoelstra (1987) using a combination of techniques in Europe, suggest such motions may be common in many locations. More measurements are necessary, but if this were found to be the case, it would be difficult to explain in terms of gravity waves since the source region would always have to be located to the east of the observation point.

Sporadic E

As was mentioned in the previous section, the only time we had enough scattering points in the lower E-region was when there was enough ionization there to get a returned signal. We interpret this ionization as a sporadic E layer that was present for much of the observation period of day 1982. Because this layer was present for

such a long period of time we are able to study its structure and characteristics by looking at the location and movement of the scattering points determined from the IMAGER system and the conventional ionogram data. Although sporadic E was present for a short period on day 177 the data record is not long enough to draw many conclusions about its structure. For this reason we limit the following dicussion to day 182.

When discussing the structure and movement of sporadic E layer we must be very careful to separate "facts" from interpretations. Toward that end, we first list key observations about the scattering points:

1) The sporadic E layer was present for the entire observation period on day 182 except for short periods when it disappeared completely.
2) Scattering points often appeared in groups of 5 to 10 points over 15 km square areas. These groups appeared in every portion of the sky during the night.
3) When a large percentage of scattering points appeared outside of 10° from zenith the peak power levels on the radar were generally below 95 dB, often below 85 dB.
4) No organized motion across the sky could be determined by comparing the location of scattering points from one sounding to the next.
5) Groups of scattering points were normally seen over five range gates (15 km).
6) The number of scattering points dropped sharply above and below the sporadic E layer.

7) The altitude having the maximum number of scattering points varied from 109 km (0418 UT) to as low as 91 km (1038 UT).

We believe the wind shear model of sporadic E formation fits the observations from day 182. The general shear conditions in the lower E region are apparently not strong enough to support a sporadic E layer by themselves, but medium scale TIDs propagating through the region enhance this general shear locally and create irregularly shaped, intense patches of sporadic E that are seen as groups of scattering points on the IMAGER and echos on the ionosonde. The layer did disappear abruptly on several occasions (0448, 0548, 0638, 0838 UT). We interpret these disappearances simply as another manifestation of the interaction between the local wind flow and propagating gravity waves. In these instances, the interactions produced shear conditions that were not strong enough to support intense patches of sporadic E or, even aided in the diffusion of existing patches.

Figure 23 illustrates the model of the partially reflecting sporadic E "layer" present on day 182. It is important to clearly define what is meant by the term "partially reflecting." Here it means both sporadic E and F region echoes are present at the same frequency on an ionogram as in Figure 24. At mid-latitude this occurs because of the geometry of a sporadic E layer as shown in Figure 23. Some of the radar energy is reflected from intense sporadic E patches while the rest never encounters these higher plasma densities until it reaches the F region. The term "partial reflection" as it is used here does not refer to a portion of the energy in an individual electromagnetic wave being reflected and a portion being transmitted; all the energy in this wave is reflected if, as the Appleton-Hartree equation

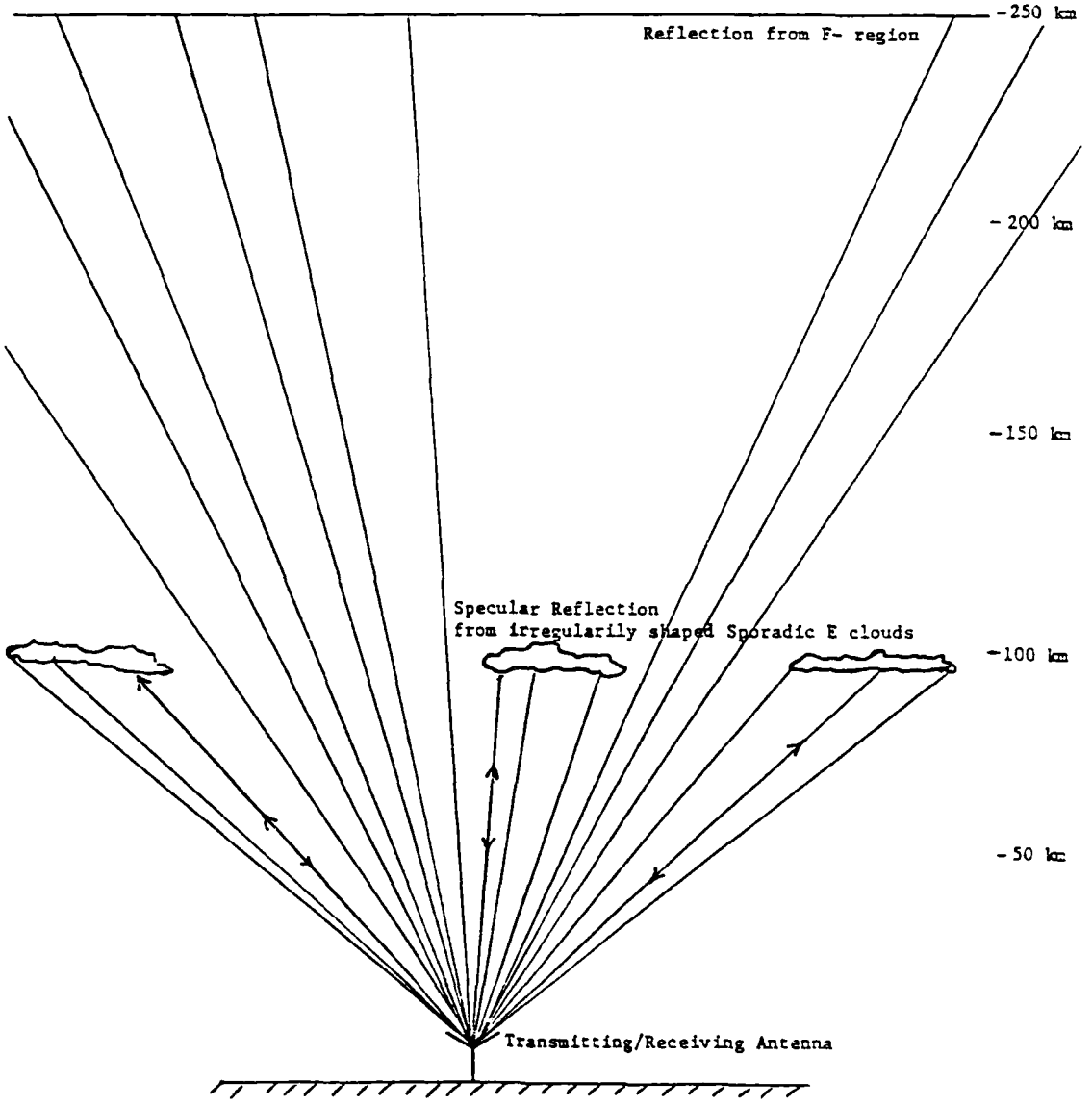

Fig. 23. Geometry of a partially reflecting sporadic E layer.

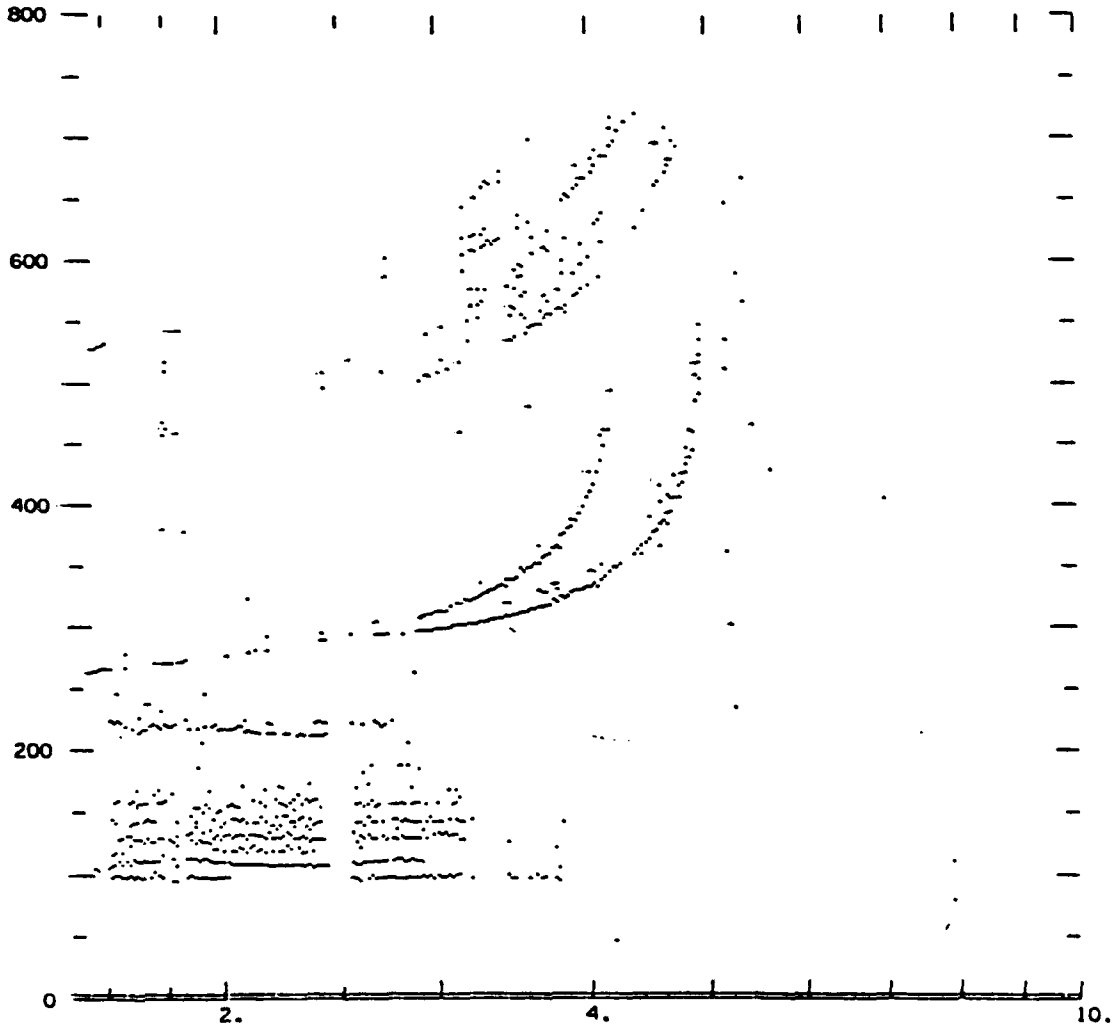

Fig. 24. Conventional ionogram from 0550 UT on Day 182.

predicts, the transmitted frequency is less than the plasma frequency.

Since we have no reason to believe otherwise, we assume these patches are equally distributed across the sky. The fact that scattering points near zenith have larger power can be explained in terms of the antenna pattern and the actual distance to the point. The antenna pattern decreases very rapidly from a maximum at zenith to a null at approximately 17° off-zenith. The $1/(\text{Radius})^2$ factor also reduces power returns as much as 20 percent for points 24° off-zenith. Figures 25a and 25b are good examples of sporadic E patches located near and off-zenith, respectively. The power profiles on the left hand side of the diagrams reflect the location of these points, the off-zenith peak powers being considerably weaker than overhead returns.

The ionograms from day 182 suggest an intriguing possibility concerning the horizontal structure of the sporadic E, namely, that the patches are occurring at regular intervals in the horizontal. If we interpret the layers near 100 km in Figure 24 as being caused by off-zenith reflections rather than variations in the vertical we get a horizontal wavelength of approximately 48 km. Skymap plots of scattering point location did not support this interpretation, with only 5 of 47 soundings indicating this might have been a possibility. Figure 26e is best of these five examples. We were limited to looking at a single wavelength in the horizontal due to radar ambiguities discussed in the previous section. With these ambiguities removed results between the two systems might agree more closely.

Since the measured velocities discussed in the previous section were consistent over time in both direction and speed, one might expect

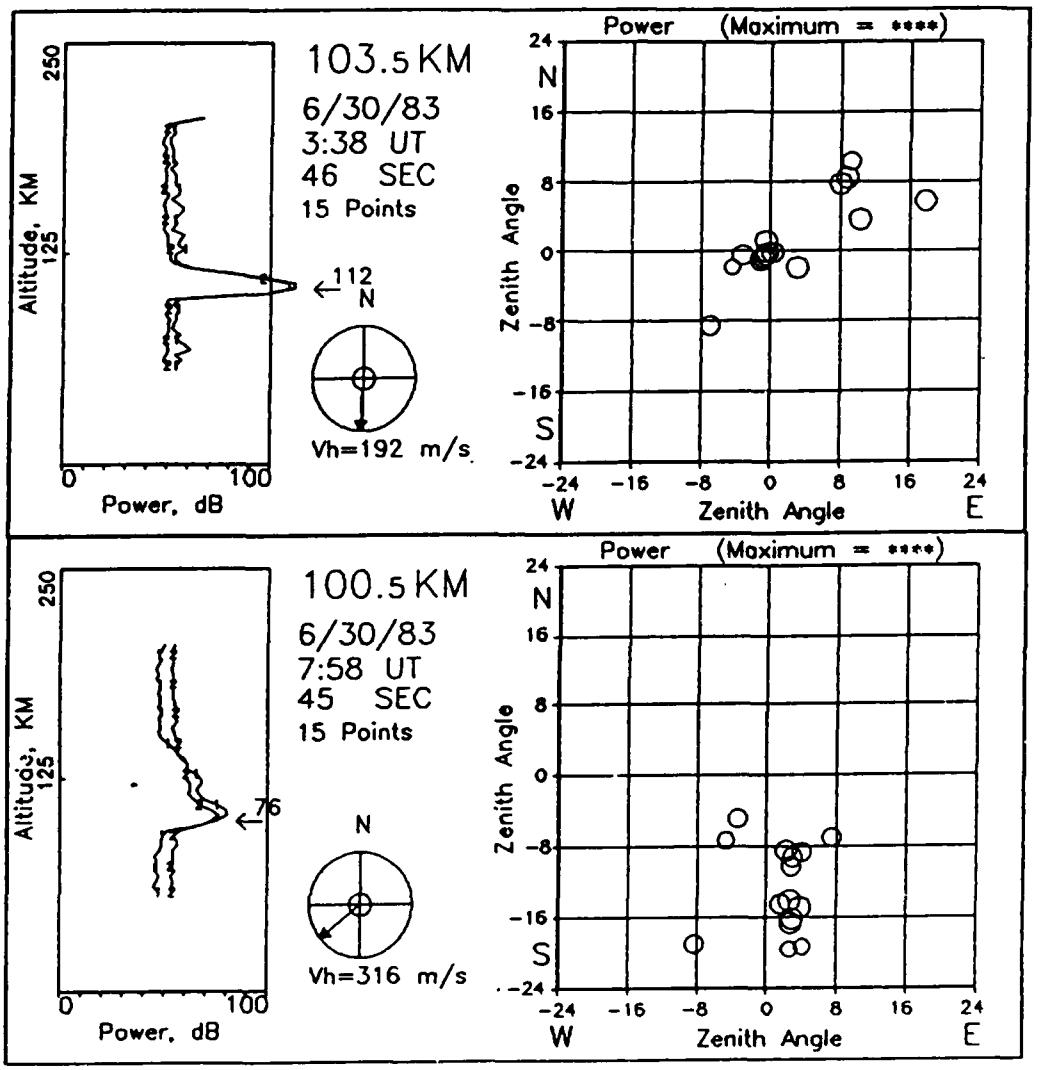

Fig. 25. Skymap plots of sporadic E patches with
(a) Intense power returns near zenith, and
(b) Weak power returns off-zenith.

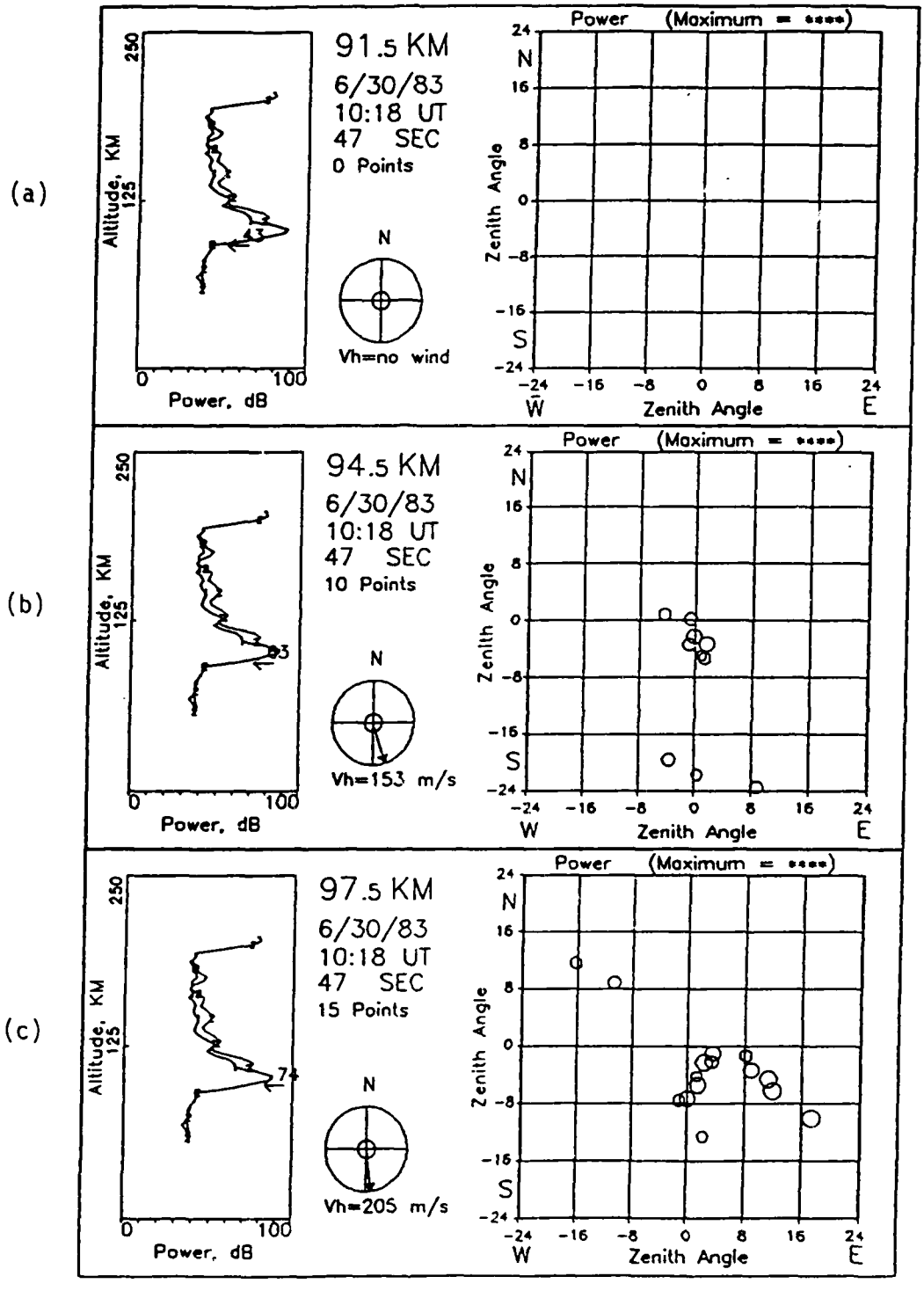

Fig. 26. Sequence of skymap plots showing vertical structure of sporadic E at 1018 UT on day 182.

(d)

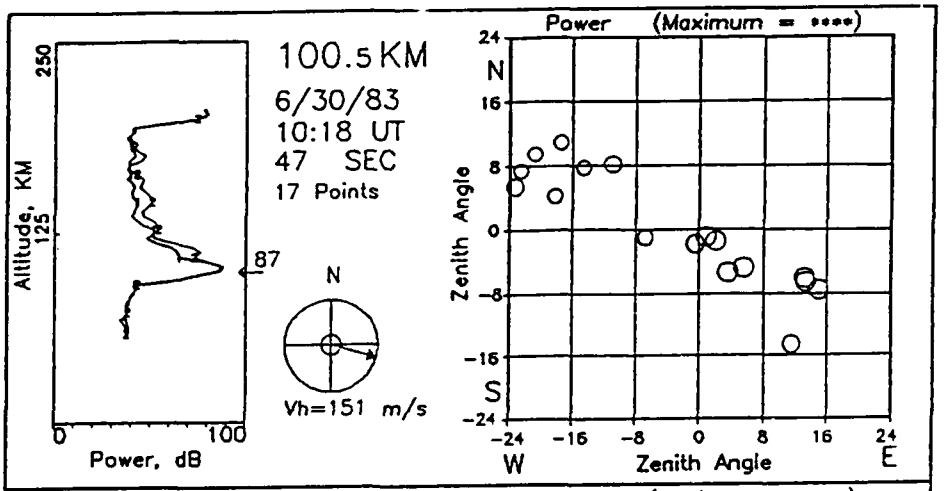

(e)

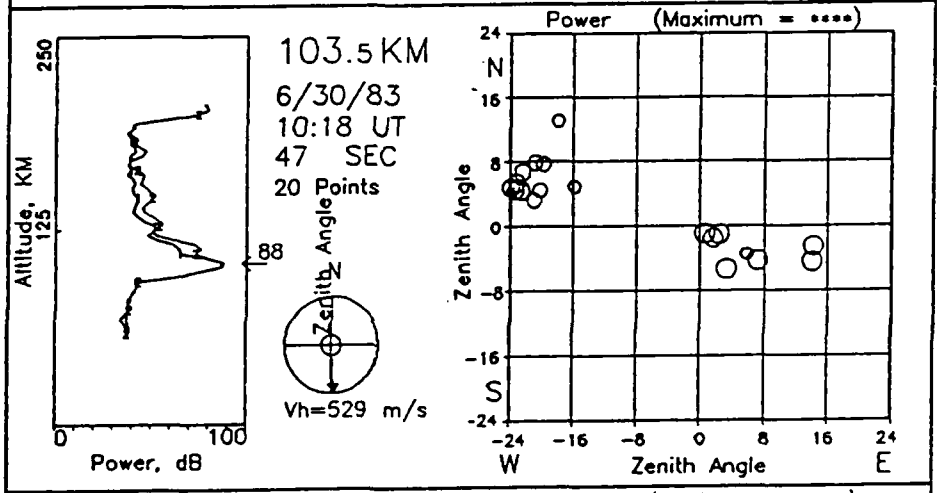

(f)

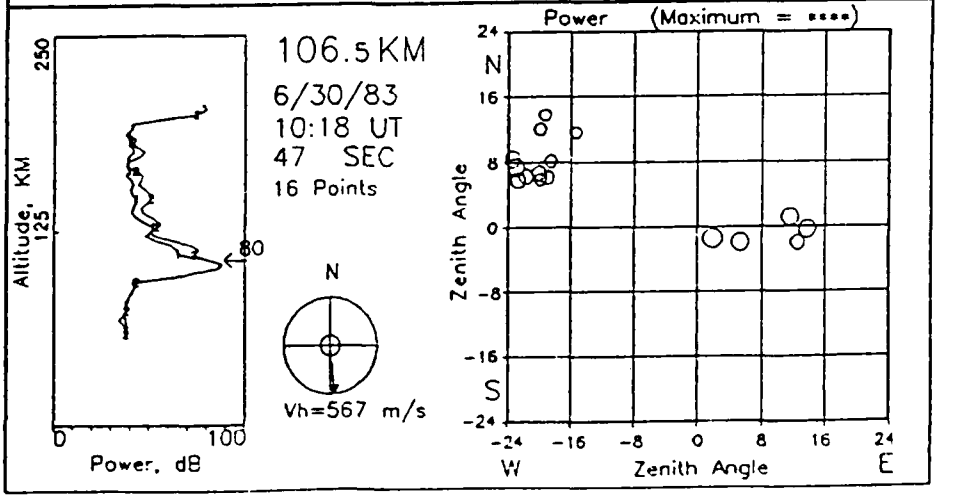

Fig. 26. (Continued)

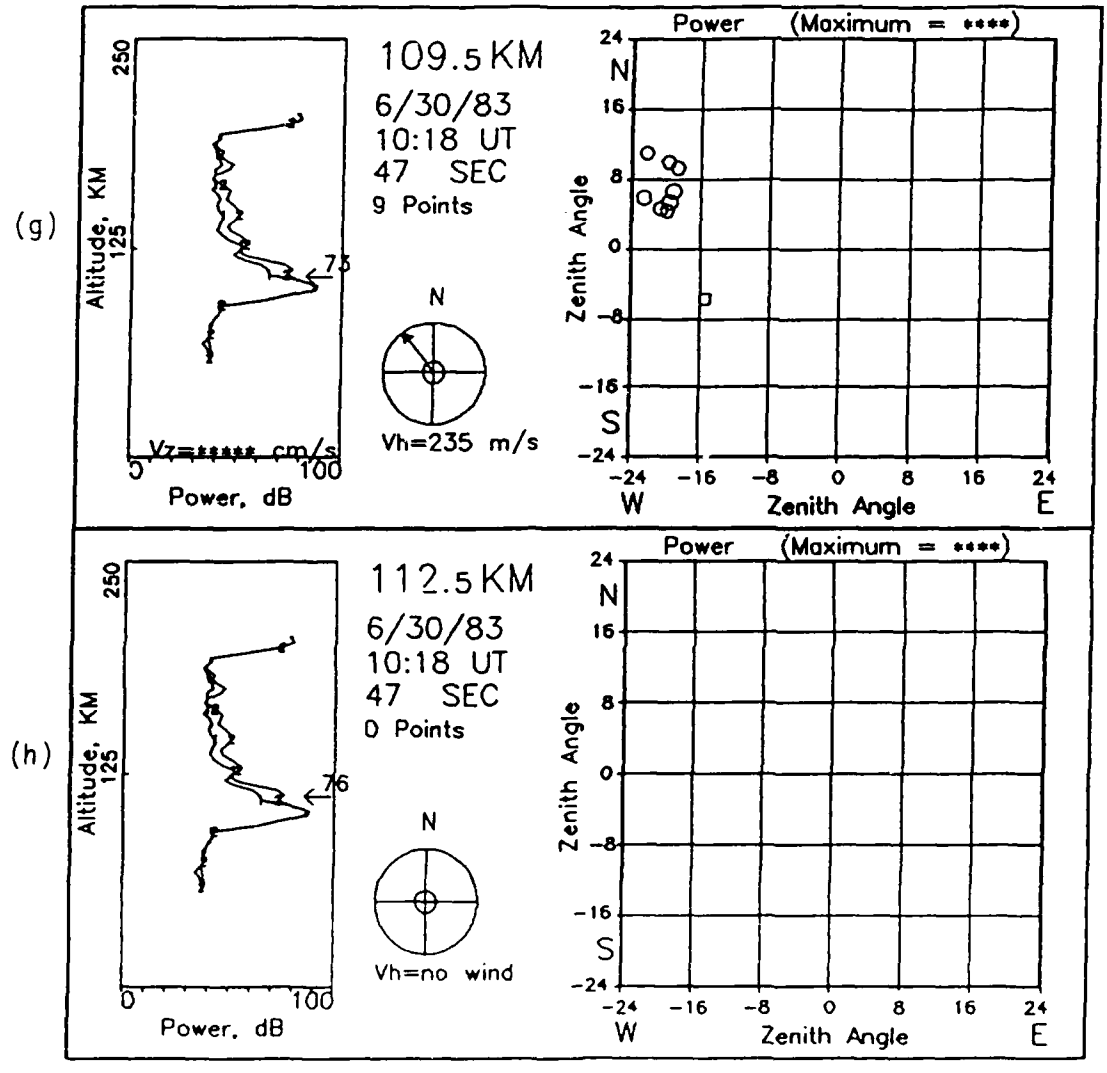

Fig. 26 (Continued)

to see a coherent pattern of scattering points moving across the sky. No such behavior was observed. Two reasons to explain this come to mind. First, in the 10 minutes between soundings, a patch moving at 200 m/s could move entirely through the unambiguous viewing region of the radar system. We would continually see new patches moving across the screen if this were the case. If the lifetime of the individual patches was less than 10 min, then sporadic E forming locally from the interaction of gravity waves with the mean flow would also appear quite randomly across the sky. Using a digital ionosonde to track the movement of sporadic E patches, Paul (1986) had similar problems even with a 6 min resolution between soundings. Better time resolution between soundings is needed to determine if either of these hypotheses are true.

Interpretation of vertical structure in the sporadic E is difficult because the radar pulselength of 4.5 km is probably greater than the layer thickness. This means the minimum thickness of a layer can't be specified more accurately than 9 km (3 range gates). Because clusters of scattering points normally appear over five range gates, we can estimate layer thickness at 6 km or less. This estimate includes irregular features on the surface of the layer which must be present since 5-10 points, rather than a single one, usually appear for every patch of sporadic E. This agrees with previous results on the thickness of sporadic E layers. A shorter pulse is needed if we are to specify thickness more accurately.

Even with the long pulselength some structure in the vertical is apparent. This is most easily seen by looking at the bottom and top of the sporadic E layer which can usually be determined to within one range gate. For example, in Figure 26 we see the base height varies

from patch to patch. In Figure 26b, the bottom edge of the patch near the zenith falls in the 94.5 km range gate. What appears to be a second distinct patch appears at 97.5 km just to the east of the first one in Figure 26c. In Figure 26d a third patch appears at 100.5 km to the northwest of the first two. This third patch then persists through 109.5 km while the first two disappear completely by 109.5 km. The sounding used in this example was not a once per night occurrence. Many other soundings showed the same thing but were less clearcut than this example.

Resolution limitations with both the ionosonde and the radar make estimating the height of the base difficult, but the layer descended approximately 10 km during the course of the night. The descent seemed to take place in two steps. Between 0318-0538 UT the base of the layer remained at approximately 106 km. At 0638 UT the sporadic E disappeared entirely only to reappear strongly 20 min later at 102 km. It remained at this level until approximately 1008 UT when it began a rapid descent down to 96 km at 1028 UT. This was the lowest altitude recorded during the entire night. From here, on the ionograms the layer ascended back up to 100 km. On the radar, judging by the number of scattering points, it appeared to continue moving downward to approximately 94 km where a very large number of scattering points (71) appeared in the very next sounding (1038 UT). These points disappeared by 1048 UT. The first descent of the layer is difficult to discuss because both instrument records (ionosonde and radar) are discontinuous because no sporadic E was present. The 0.3 km/min rate of descent between 1008-1028 UT is similar to descending layer rates reported by Miller and Smith (1978) which they described in terms of Axford's 'corkscrew' mechanism.

While the descent rates are similar the starting points are quite different, their's beginning its descent at 125 km and ours starting at only 102 km.

Atomic Oxygen Emissions at 557.7 nm

In terms of optical emissions (OH and O) from the lower thermosphere, day 182 was the most active day during the two week MAPSTAR campaign. It seems more than coincidence that the occurrence of sporadic E, at roughtly the same altitude as 557.7 nm emissions, peaked on the same night. In what ways can we compare the two phenomena? We have already considered sporadic E and found that when it was present we could determine velocities over a 20 km range in the lower thermosphere. From the discussion in the previous section we also saw the sporadic E exhibited a marked periodicity during the night. With photometer equipment at both Boot Lake and Jelm we are able to examine these same characteristics using 557.7 nm atomic oxygen emissions.

Day 182 results (J.W. Meriwether, private communication, 1986) using the 5-point tilting-filter photometer system at Boot Lake are shown in Figures 27 and 28. Figure 27 shows the normalized intensity traces for the south, zenith, and north directions; Figure 28 shows similar curves for the west, zenith, and east directions. In each case the lower two curves have been offset by 0.2 and 0.4, respectively, so the results could be clearly seen on the diagram.

It is obvious from the successive time lags between the curves in Figure 27 that the major features have a nearly constant northward component of motion for much of the night. The major features in Figure 28 are stacked on top of each other; for this reason we conclude there

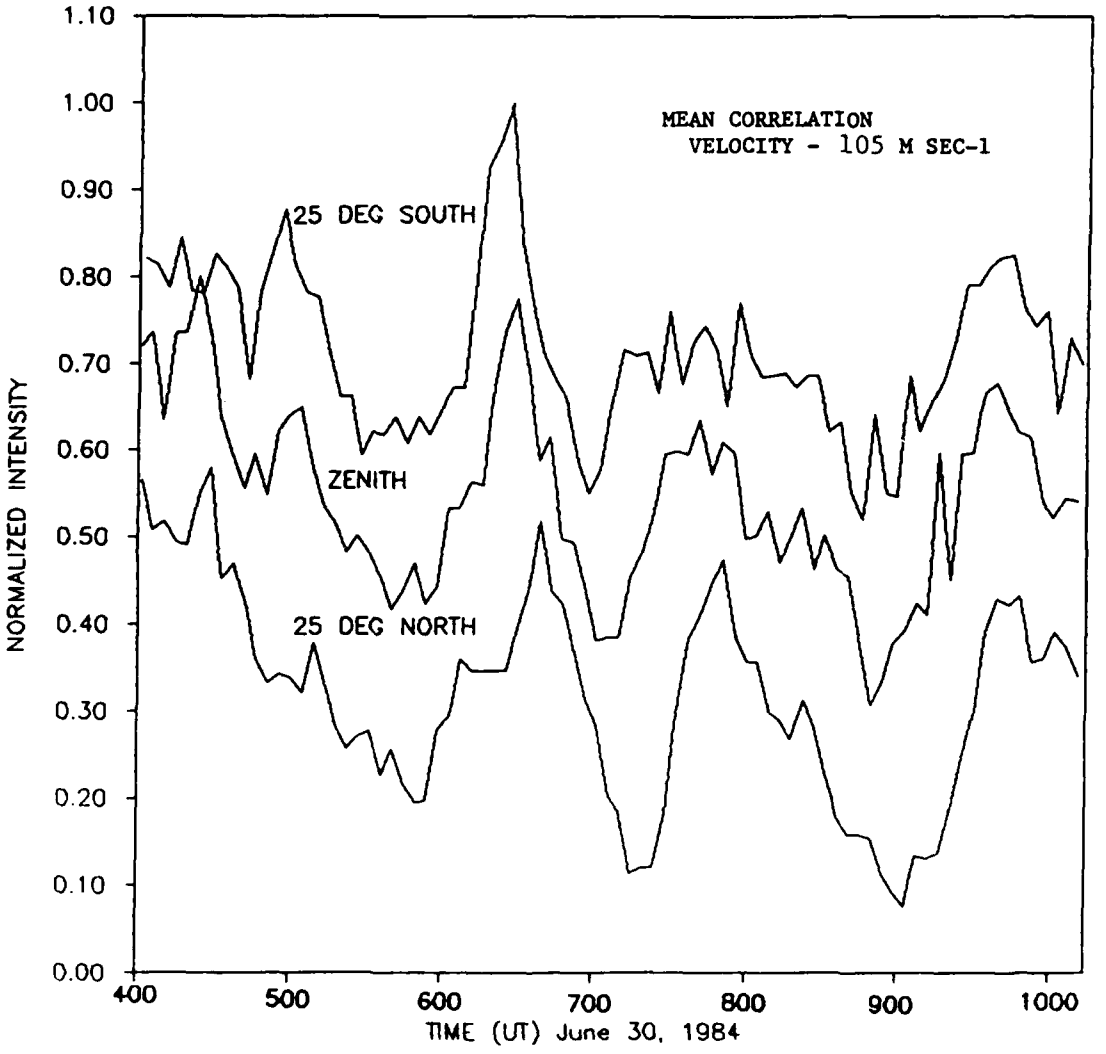

Fig. 27. Boot Lake, CO north-zenith-south 557.7 nm atomic oxygen intensity profiles (Day 182).

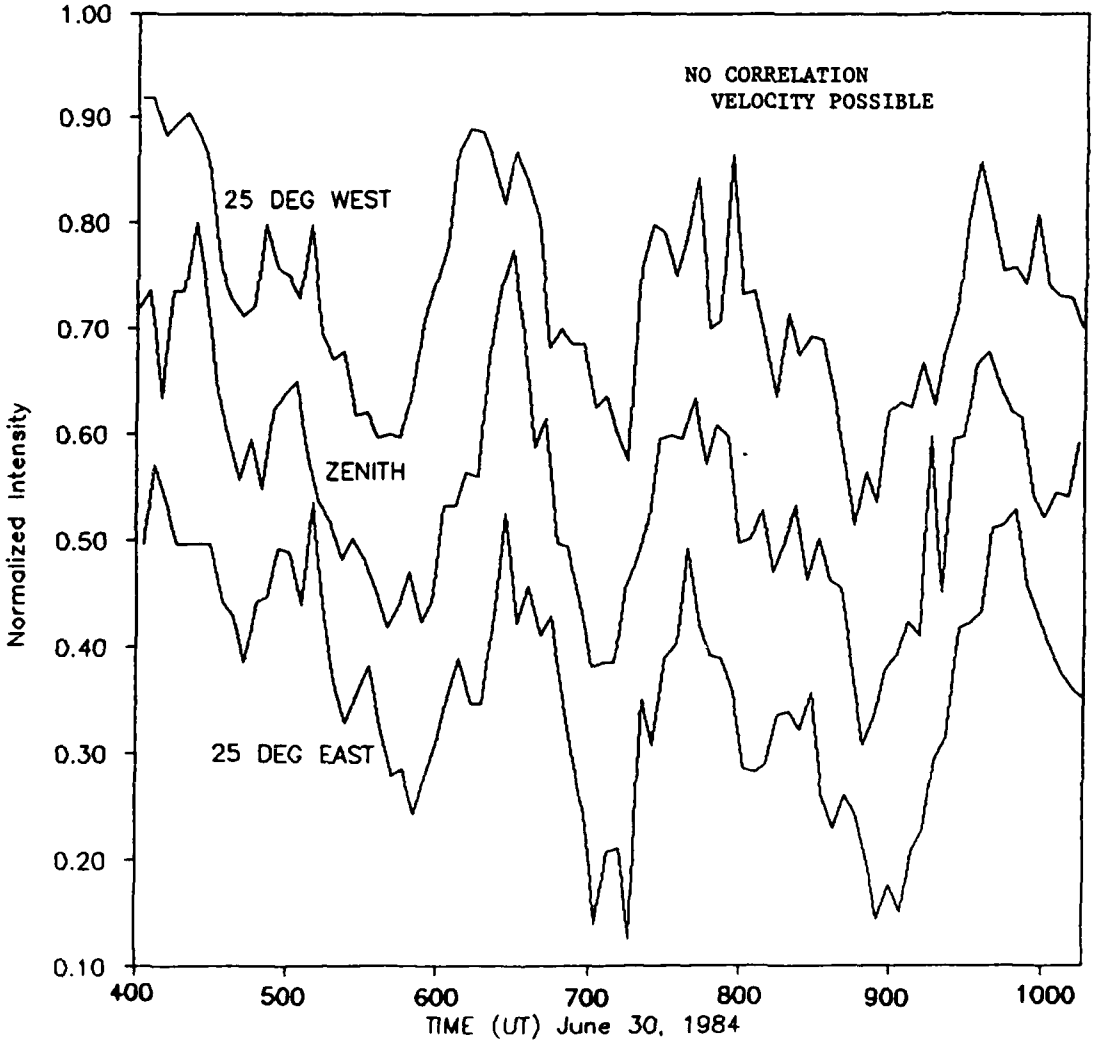

Fig. 28. Boot Lake, CO east-zenith-west 557.7 nm atomic oxygen intensity profiles (Day 182).

is little or no motion in the east-west direction. By taking the average time difference between the major features and dividing by the distance separating the observation points (44.2 km from zenith to 25° off zenith if we assume the emissions are from 95 km) we arrive at a "mean correlation velocity" of 105 m/s toward the north.

A mean correlation velocity of 95 m/s was also obtained by comparing the Boot Lake intensity curves to the Polaris imaging curves (A. W. Peterson, private communication, 1987) from the Jelm site. The distance between the zenith viewing point at Boot Lake and the Polaris monitoring point at Jelm is approximately 241 km. Because of the great distance between these two points, we were only able to use the major peak and major trough sequence seen during the night to calculate this correlation velocity (see Figure 29). The other features on the curves in Figure 29 were generally similar but they were not distinct enough to consider in the velocity calculation.

Others have seen similar motions in the 557.7 nm green line emissions (Freund and Jacka, 1979; Meek and Manson, 1983) and have described these drifts in terms of the phase velocity of gravity waves moving through the region. We favor this interpretation here. If these motions represented the neutral wind they would exhibit a clockwise change in direction with time. No such change is apparent throughout the entire observation period.

If these drift motions represent gravity waves, we are hardpressed to identify an apparently continuous source to the south of Boot Lake. Review of Figures 17-19 eliminates thunderstorms, jetstreams, and mountain lee waves as lower atmospheric sources. Auroral activity can be eliminated based on the drift direction; the breaking of tidal

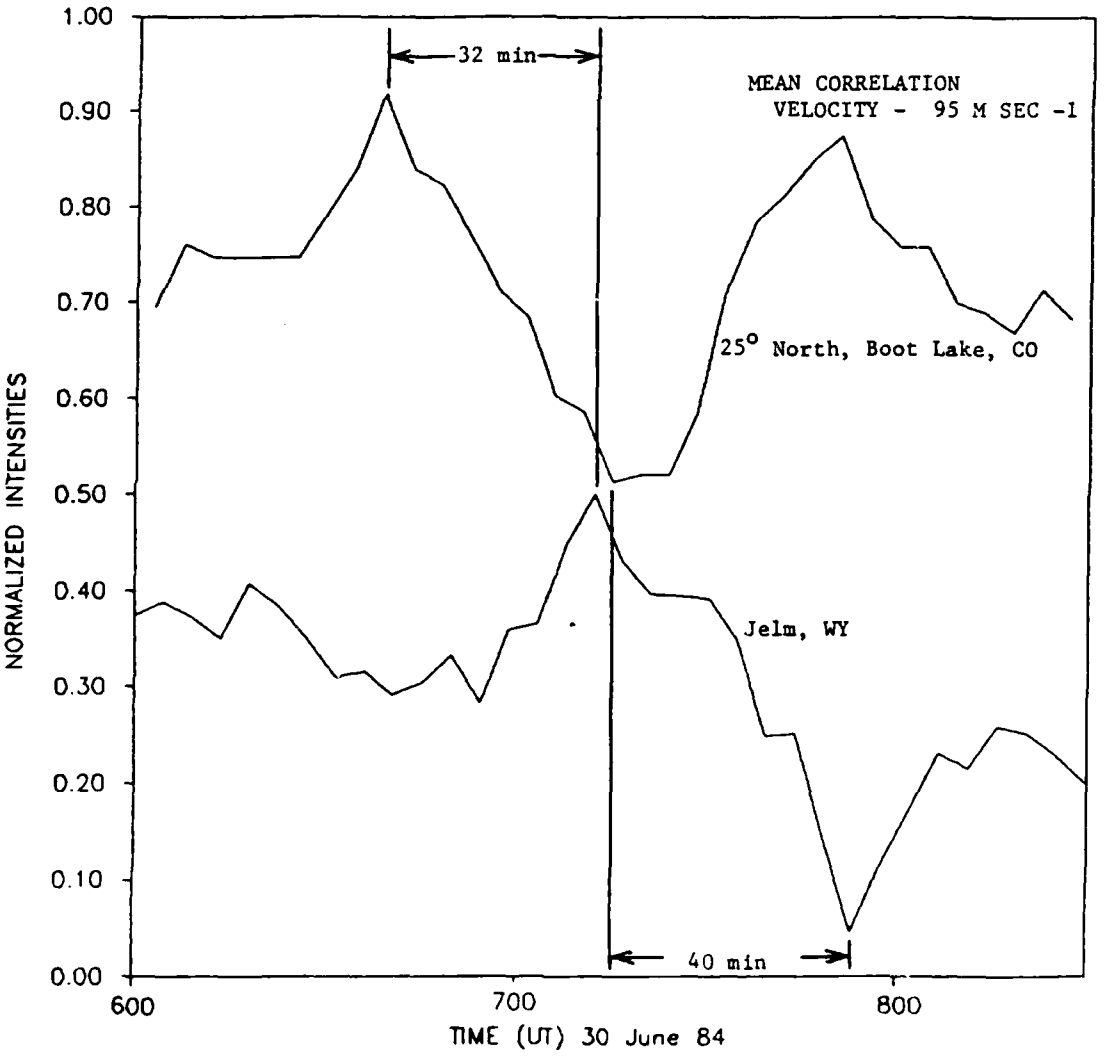

Fig. 29. Boot Lake, CO zenith and Jelm, WY Polaris 557.7 nm atomic oxygen traces (Day 182).

waves in the mesosphere would produce a clockwise shift in direction similar to the shift in the neutral wind.

At this point we have two sets of observations showing velocities directed in nearly opposite directions. Could these two processes, sporadic E formation and 557.7 nm oxygen emissions, be driven by different components of the gravity wave spectrum? Because the wind shear theory of sporadic E formation depends on the orientation of the magnetic field it is plausible that one direction of propagation would produce sporadic E and not another. However, in the case of oxygen emission the magnetic field plays no role; it is only changes in density that enhance or reduce the emissions. This process should "see" gravity waves propagating in any direction and respond accordingly.

The 557.7 nm green line intensities and the sporadic E both showed strong periodicities. With such widely varying results in the directions of motion one might expect these periodicities would not resemble each other very closely. This is indeed the case as can be seen in Figure 30 where we plot the normalized spectral densities versus the periods. Only periods greater than 20 min have been depicted here since this corresponds to the Nyquist frequency limit for the sporadic E curve, above which aliasing occurs. Neither have we considered periods greater than 180 min as this begins to approach the tidal wave periods in the atmosphere. As can be seen in the diagram the sporadic E has a strong peak at 57.5 minutes while the green line intensities peak at approximately 100 min. The rest of the curves are also dissimilar with peaks in one occurring at minima in the other.

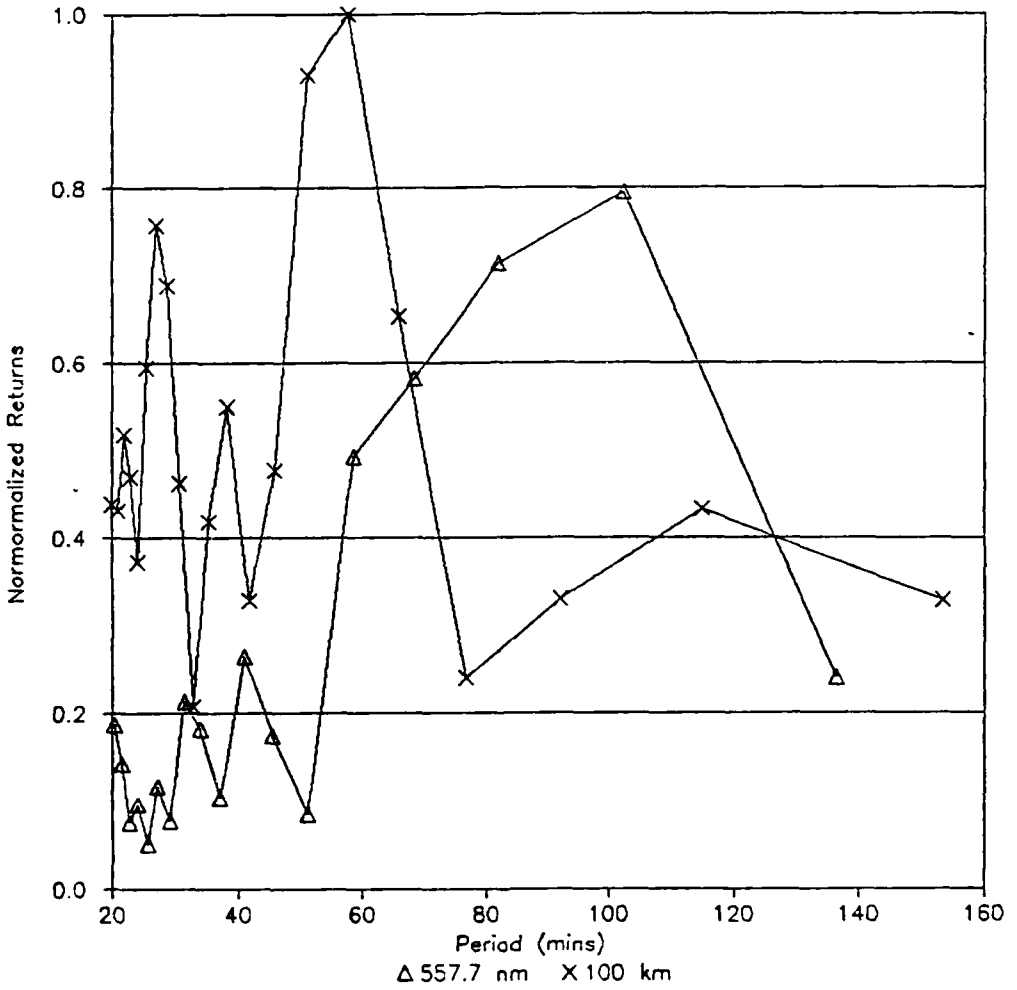

Fig. 30. Power spectral density curves for 557.7 nm atomic oxygen at Boot Lake, CO and received power on Doppler interferometer (Day 182).

CHAPTER V

CONCLUSIONS

There has been considerable debate about the proper interpretation of apparent-motion vectors determined from Doppler shifts of the returned radar pulses. We used a 2.66 MHz Doppler interferometer radar to obtain these apparent-motion vectors in the lower E region. On two separate occasions, totaling over 10 hours of observation, the apparent-motion vectors were between 160 and 325 m/s. On both occasions the direction of motion through a 20 km deep layer was toward the west with some variation on either side of this. We interpret these results as being horizontal phase motions of gravity waves moving through the lower E region. First, the magnitude of the velocities is too large by at least a factor of 2 for these to be considered bulk wind velocities. Indeed, the velocities fit very nicely into the medium scale TID range identified by Georges (1968). Second, if these were neutral winds we would expect them to change direction with altitude over a 10 km range (one half the vertical wave-length) or less. This was not apparent during the observation period. Finally, if these motions represented neutral winds they would also be expected to rotate clockwise in time with the diurnal or semidiurnal tide. There was no evidence of this occurring.

Because the direction of these motions was consistently from a small range of azimuths during each of the observation periods, we were able to identify possible sources in the lower atmosphere. In

one case, large low pressure troughs were proposed as the source regions for gravity waves. In the second case, thunderstorms were suggested as the source for propagating gravity waves.

The long term presence of the sporadic E layer on day 182 also made it possible to examine the horizontal, and to some extent the vertical, structure of the layer. The structure of the sporadic E layer appears to be similar to the observations reported by Miller and Smith (1978), in particular:

1) The partially reflecting sporadic E "layer" appears to be made of distinct patches separated by areas of very weak ionization.
2) The sporadic E patches are quite irregular in shape as clusters of scattering points appear instead of a single specularly reflected point as would be expected from a smooth layer.
3) The bases and tops of individual sporadic E patches varied considerably, in one case by as much as 6 km.

We found little support for regularly spaced corrugations in the E region surface as the layering on the ionograms suggests. Instead the patches seem to be individual scattering centers located about the sky in random fashion.

Drift velocities and spectral power density curves were calculated for the 557.7 nm atomic oxygen emission curves on day 182. These were compared to the Doppler interferometer results and found to be significantly different in both cases. The drift velocities calculated from the emission curves showed horizontal motion toward the north for virtually the entire observation period. This is 90° or more from the

direction of the horizontal velocities calculated from the radar data. The spectral power density curves also showed little connection between the two processes. The dominant period seen on the radar was approximately one hour; for the emission data, near 100 min.

The first of these findings was somewhat surprising given the fact the two processes are occurring at virtually the same altitude. We have no theories as to why there is such a discrepancy between these measurements. The second result was somewhat less surprising considering the great differences in the processes responsible for the phenomena, one being tied to the movement of ions along the magnetic field line, the other involving chemical processes dependent on the amount of convergence forced on the constituents by shears in the wind field.

Recommendations for Futher Research

More research must be done before there is conclusive proof that we are measuring phase motions associated with propagating gravity waves. The Doppler interferometer system shows great promise in being able to sort this out. We discuss below several specific recommendations for follow-on research efforts.

Data must be collected continuously over a much longer period, including daylight operation, if we hope to answer the following questions: Were the large apparent-velocities associated with the sporadic E, or is this high-speed phenomenon there all the time? Does the direction vary through 360° or is there really a lack of eastward motion? Does the direction of the apparent-velocity correlate with suspected lower atmospheric sources for gravity waves? With auroral sources? With tidal motions?

Individual soundings must include more pulse-sets and be taken more often. Suggested values are 512 pulses/pulse-set with soundings every 2 min. The first of these recommendations would add more low frequency components to the velocity calculation. Would this additional low frequency contribution bring the calculated horizontal velocities down to neutral wind values? The second recommendation would help in determining the origin of sporadic E. Do patches form and dissipate in a single location or do they move across the sky? How rapidly does this formation process take place?

Running the radar in conjunction with the 5-point imaging photometer should be considered at every opportunity. It will take several more campaigns with extremely active days similar to day 182 to tell whether the large differences in velocity between the two systems occur on a regular basis or not. Greater time resolution on the 557.7 nm measurements should also be attempted. This should be possible given the automation built into the photometer system. With greater time resolution more accurate horizontal drift motions could be determined.

Several other questions come to mind. We have said the apparent-velocities do not represent neutral wind motions. Can a technique be developed that would definitively determine this to be true? The mass continuity equation (equation 2.3) offers a starting point for such a test. If the local rate of change of density is neglected, all that remains are the divergence terms. Each of these can be measured if there are enough points spread about the sky at each level, with the sum being zero if the components represent bulk wind motions. If they represent phase motions the results are likely to be quite different than zero. If it were determined these were phase velocities, a

second question comes to mind, "Could a technique be developed to separate phase motions from bulk motions since both these quantities are likely to be part of the result?" Little has been said about the horizontal and vertical wavelengths of the gravity waves moving through the region. Can these be calculated from the motions measured on the radar system?

Almost all of these recommendations could be implemented with a faster more reliable Doppler interferometer system. Just such a system is being built. The results will provide a wealth of new information on the mesosphere and lower thermosphere and should enable us to answer some of the questions raised in this report.

AD-A186 126 AN ANALYSIS OF APPARENT-MOTION VECTORS IN AND THE STRUCTURE OF A MID-LATI..(U) AIR FORCE INST OF TECH WRIGHT-PATTERSON AFB OH T D HALDERMAN 1987 2/2

UNCLASSIFIED AFIT/CI/NR-87-102T F/G 4/2 NL

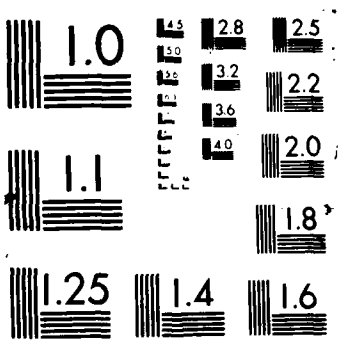
1.0
1.1
1.25
1.4
1.6
1.8
2.0
2.2
2.5
2.8
3.2
3.6
4.0

REFERENCES

Adams, G. W., J. W. Brosnahan, T. D. Halderman, A. W. Peterson, T. -F. Tuan, J. W. Meriwether, L. L. Cogger, D. J. Baker, W. R. Pendleton, P. M. Espy, and R. A. Armstrong, Radar and optical observations of mesospheric structures, unpublished manuscript, November 18, 1986a.

Adams, G. W., J. W. Brosnahan, D. C. Walden, and S. F. Nerney, Mesospheric observations using a 2.66 MHz radar as an imaging Doppler interferometer: Description and first results, Journal of Geophysical Research, 91(A2), 1671-1683, 1986b.

Adams, G. W., D. P. Edwards, and J. W. Brosnahan, The imaging Doppler interferometer: Data analysis, Radio Science, 20, 1481-1492, 1985.

Adams, G. W., A. W. Peterson, J. W. Brosnahan, and J. W. Neuschaefer, Radar and optical observation of mesospheric wave activity during the lunar eclipse of 6 July 1982, unpublished manuscript, February 14, 1987.

Armstrong, E. B., The association of visible airglow features with a gravity wave, Journal of Atmospheric and Terrestrial Physics, 44, 325-336, 1982.

Axford, W. I., The formation and vertical movement of dense ionized layers in the ionosphere due to neutral winds, Journal of Geophysical Research, 68, 769-779, 1963.

Axford, W. I. and D. M. Cunnold, The wind-shear theory of temperate zone sporadic E, Radio Science, 1, 191-198, 1966.

Balsley, B. B., A. Rey, and R. F. Woodman, On the plasma instability mechanisms responsible for Es_q, Journal of Geophysical Research, 81, 1391-1396, 1976.

Barth, C. A. and A. F. Hildebrandt, The 5577 A airglow emission mechanism, Journal of Geophysical Research, 66, 985-986, 1961.

Battaner, E. and A. Molina, Turbopause internal gravity waves, 557.7 nm airglow, and eddy diffusion coefficients, Journal of Geophysical Research, 85(A12), 6803-6810, 1980.

Bedinger, J. F., H. B. Kneflich, E. Manring, and D. Layzer, Upper-atmosphere winds and their interpretation - 1. Evidence for strong nonlinearity of the horizontal flow above 80 km, Planetary Space Science, 16, 159-195, 1968.

Beer, T., Atmospheric Waves, Adam Hilger, London, 1974.

Bowman, G. G., Traveling ionospheric disturbances associated with ionospheric storms, Journal of Atmospheric and Terrestrial Physics, 27, 1247-1261, 1965.

Bowman, G. G., Movements of ionospheric irregularities and gravity waves, Journal of Atmospheric and Terrestrial Physics, 30, 721-734, 1968.

Chan, K. L. and O. G. Villard, Jr., Observation of large-scale traveling ionospheric disturbances by spaced-path high-frequency instantaneous-frequency measurements, Journal of Geophysical Research, 67, 973-988, 1962.

Chapman, S., Some phenomena of the upper atmosphere, Proceedings of the Royal Society of London, A132, 353-374, 1931.

Chapman, S. and R. S. Lindzen, Atmospheric Tides, Gordon and Breach Science Publishers, New York, 1970.

Chimonas, G. and W. I. Axford, Vertical movement of temperate-zone sporadic E layers, Journal of Geophysical Research, 73, 111-117, 1968.

Coble, B. B., Middle atmospheric wind measurements using a medium frequency radar, Master's Thesis, Soil Science and Biometeorology Department, Utah State University, 1987 (available as CASS Report GR-07).

Davies, K., Ionospheric Radio Propagation, Dover Publications, Inc., New York, 1966.

Davies, K. and J. E. Jones, Three-dimensional observations of traveling ionospheric disturbances, Journal of Atmospheric and Terrestrial Physics, 33, 39-46, 1971.

Davies, K. and J. E. Jones, Ionospheric disturbances produced by severe thunderstorms, NOAA Professional Paper #6, United States Department of Commerce, Rockville, Maryland, December, 1972.

Donahue, T. M., B. Guenther, and R. J. Thomas, Ogo 6 airflow observations, Journal of Geophysical Research, 79, 6662-6689, 1973.

Dungey, J. W., The influence of the geomagnetic field on turbulence in the ionosphere, Journal of Atmospheric and Terrestrial Physics, 8, 39-42, 1956.

Dungey, J. W., Effect of a magnetic field on turbulence in an ionized gas, Journal of Geophysical Research, 64, 2188-2191, 1959.

Francis, S. H., Theory and models of atmospheric acoustic-gravity waves and traveling ionospheric disturbances, Joint Radar Propagation Study, Bell Laboratories, Wippany, New Jersey, 1973.

Freund, J. T. and F. Jacka, Structure in the 557.7 nm [01] airglow, Journal of Atmospheric and Terrestrial Physics, 41, 25-31, 1979.

Georges, T. M., HF Doppler studies of traveling ionospheric disturbances, Journal of Atmospheric and Terrestrial Physics, 30, 735-746, 1968.

Goodwin, G. L., The dimensions of some horizontally moving Es region irregularities, Planetary Space Science, 14, 759-771, 1966.

Goodwin, G. L., Some horizontally-moving ionospheric irregularities at high latitudes, Planetary Space Science, 16, 273-283, 1968.

Gross, S. H., Large scale waves and quasi-stationary structures (abstract), Eos Transactions, American Geophysical Union, 64, 274, 1983.

Grubb, R. N., The NOAA SEL HF Radar System (Ionospheric Sounder), NOAA Technical Memorandum ERL-55, United States Department of Commerce, Boulder, Colorado, October, 1979.

Hargreaves, J. K., The Upper Atmosphere and Solar-Terrestrial Relations: An Introduction to the Aerospace Environment, Van Nostrand Reinhold, New York, 1979.

Hines, C. O., Internal atmospheric gravity waves at atmospheric heights, Canadian Journal of Physics, 38, 1441-1481, 1960.

Hines, C. O., The upper atmosphere in motion, Quarterly Journal of the Royal Meteorological Society, 89, 1-42, 1963.

Hines, C. O., Diurnal tide in the upper atmosphere, Journal of Geophysical Research, 71, 1453-1459, 1966.

Hines, C. O., Possible sources of waves in noctilucent clouds, Paper No. 22 in, The Upper Atmosphere in Motion, Heffernan Press, Worcester, Massachusetts, 1974a.

Hines, C. O., Propagation velocities and speeds in ionospheric waves: A review, Journal of Atmospheric and Terrestrial Physics, 36, 1179-1204, 1974b.

Hunsucker, R. D., Chatanika radar investigation of high latitude E region ionization structure and dynamics, Radio Science, 10, 277-288, 1975.

Hunsucker, R. D. and L. H. Tveten, Large traveling-ionospheric-disturbances observed at mid-latitudes utilizing the high resolution h.f. backscatter technique, Journal of Atmospheric and Terrestrial Physics, 29, 909-916, 1967.

Kelder, H., and T. A. Th. Spoelstra, Medium scale TIDs observed by radio interferometry and differential Doppler techniques, Journal of Atmospheric and Terrestrial Physics, 49, 7-17, 1987.

Kochansky, A., Atmospheric motions from sodium cloud drifts, Journal of Geophysical Research, 69, 3651-3662, 1964.

Leighton, H. I., A. H. Shapley, and E. K. Smith, The occurrence of sporadic E during the IGY, in Ionospheric Sporadic E, The Macmillen Company, New York, 1962.

Lindzen, R. S., The application of classical atmospheric tidal theory, Proceedings of the Royal Society of London, A303, 299-316, 1968.

Mayr, H. G., I. Harris, F. Varosi, and F. A. Herrero, Global excitation of wave phenomena in a dissipative multiconstituent medium - 2. Impulsive perturbations in the earth's ionosphere, Journal of Geophysical Research, 89(A12), 10961-10986, 1984.

Meek, C. E., and A. H. Manson, Measurements of the structure and drift velocities of airglow (λ = 557.7 nm) irregularities: Saskatoon (52° N, 107° W), Canada, Journal of Atmospheric and Terrestrial Physics, 45, 203-212, 1983.

Meek, C. E., I. M. Reid, and A. H. Manson, Observation of mesospheric wind velocities. I. Gravity wave horizontal scales and phase velocities determined from spaced wind observations, Report No. 1, Institute of Atmospheric and Space Science, University of Saskatchewan, Saskatoon, Saskatchewan, 1985.

Mercier, C., Observation of atmospheric gravity waves by radio-interferometry, Journal of Atmospheric and Terrestrial Physics, 48, 605-624, 1986.

Meriwether, J. W. Jr., C. A. Tepley, S. A. Price, P. B. Hayes, and L. L. Cogger, Remote ground-based observations of terrestrial airglow emissions and thermospheric dynamics at Calgary, Alberta, Canada, Optical Engineering, 22, 128-132, 1983.

Miller, K. L. and L. G. Smith, Horizontal structure of mid-latitude sporadic E layers observed by incoherent scatter radar, Radio Science, 10, 271-276, 1975.

Miller, K. L. and L. G. Smith, Incoherent scatter radar observations of irregular structure in mid-latitude sporadic E layers, Journal of Geophysical Research, 83, 3761-3775, 1978.

Moreels G. and H. Herse, Photographic evidence of waves around the 85 km level, Planetary Space Science, 25, 265-273, 1977.

Munro, G. H., Short-period changes in the F region of the ionosphere, Nature, 162, 886, 1948.

Munro, G. H., Traveling disturbances in the ionosphere, Proceedings of the Royal Society of London, A219, 208-223, 1950.

Munro, G. H., Traveling ionospheric disturbances in the F region, Australian Journal of Physics, 11, 91-112, 1968.

Narcisi, R. S., Processes associated with metal-ion layers in the E region of the ionosphere, Space Research, 8, 360-369, 1968.

Paul, A. K., Limitations and possible improvements of ionospheric models for radio propagation: Effects of sporadic E layers, Radio Science, 21, 304-308, 1986.

Petitdidier M. and H. Teitelbaum, Lower thermospheric emissions and tides, Planetary Space Science, 25, 711-721, 1977.

Riggin, D., W. E. Swartz, J. Providakes, and D. T. Farley, Radar studies of long-wavelength waves associated with mid-latitude sporadic E layers, Journal of Geophysical Research, 91(A7), 8011-8024, 1986.

Rosenberg, N. W., Statistical analysis of ionospheric winds - II., Journal of Atmospheric and Terrestrial Physics, 30, 907-917, 1968.

Rowe, J. F. Jr., Downward transport of nighttime Es layers into the lower E region at Arecibo, Journal of Atmospheric and Terrestrial Physics, 36, 225-236, 1974.

Slanger, T. G. and G. Black, O(^{1}S) in the lower thermosphere - Chapman vs Barth, Planetary Space Science, 25, 79-88, 1977.

Smith, L. G. and A. E. Mechtly, Rocket observations of sporadic E layers, Radio Science, 7, 367-376, 1972.

Tedd, B. L. and M. G. Morgan, TID observations at spaced geographic locations, Journal of Geophysical Research, 90(A12), 12307-12319, 1985.

Thome, G. D., Incoherent scatter observation of traveling ionospheric disturbances, Journal of Geophysical Research, 69, 4047-4049, 1964.

Titheridge, J. E., Periodic disturbances in the ionosphere, Journal of Geophysical Research, 73, 243-252, 1968.

Turek, R. S., An analysis of upper atmospheric parameters derived from the observation of meteor echoes by a 2.66 MHz radar, Master's Thesis, Soil Science and Biometeorology Department, Utah State University, 1986 (available as CASS Report GR-06).

van Eyken, A. P., P. J. S. Williams, A. D. Maude, and G. Morgan, Atmospheric gravity waves and sporadic E, Journal of Atmospheric and Terrestrial Physics, 44, 25-29, 1982.

Vincent, R. A., Ionospheric irregularities in the E region, Journal of Atmospheric and Terrestrial Physics, 34, 1881-1898, 1972.

Vincent, R. A. and I. M. Reid, HF Doppler measurements of mesospheric gravity wave momentum fluxes, Journal of the Atmospheric Sciences, 40, 1321-1333, 1983.

Waldock, J. A. and T. B. Jones, HF Doppler observations of medium-scale traveling ionospheric disturbances at mid-latitudes, Journal of Atmospheric and Terrestrial Physics, 48, 245-260, 1986.

Whitehead, J. D., The formation of the sporadic E layer in the temperate zones, Journal of Atmospheric and Terrestrial Physics, 20, 49-58, 1961.

Whitehead, J. D., Production and prediction of sporadic E, Reviews in Geophysics and Space Physics, 8, 65-144, 1970.

Whitehead, J. D., Difficulty associated with wind shear theory of sporadic E, Journal of Geophysical Research, 76, 3127-3136, 1971.

Wright, J. W. and L. S. Fedor, The interpretation of ionospheric radio drift measurements - II. Kinesonde observation of microstructure and vertical motion in sporadic E, Journal of Atmospheric and Terrestrial Physics, 31, 925-942, 1969.

Wright, J. W., C. H. Murphy, and G. V. Bull, Sporadic E and the wind structure of the E region, Journal of Geophysical Research, 72, 1443-1460, 1967.

Young, J. M., C. Y. Johnson, and J. C. Holmes, Positive ion composition of a temperate-latitude sporadic E layer as observed during a rocket flight, Journal of Geophysical Research, 72, 1473-1479, 1967.

Zbinden, P. A., M. A. Hidalgo, P. Eberhardt, and J. Geiss, Mass spectrometer measurements of the positive ion composition in the D and E regions of the ionosphere, Planetary Space Science, 23, 1621-1642, 1975.

END

12-87

DTIC